

Fault-Tolerant Preparation of Quantum Polar Codes Encoding One Logical Qubit

Ashutosh Goswami¹, Mehdi Mhalla², Valentin Savin¹

¹ Univ. Grenoble Alpes, CEA-Léti, F-38054 Grenoble, France

² Univ. Grenoble Alpes, CNRS, Grenoble INP, LIG, F-38000 Grenoble, France

ashutosh-kumar.goswami@cea.fr, mehdi.mhalla@univ-grenoble-alpes.fr, valentin.savin@cea.fr

September 15, 2022

Abstract

This paper explores a new approach to fault-tolerant quantum computing, relying on quantum polar codes. We consider quantum polar codes of Calderbank-Shor-Steane type, encoding one logical qubit, which we refer to as Q_1 codes. First, we show that a subfamily of Q_1 codes is equivalent to the well-known family of Shor codes. Moreover, we show that Q_1 codes significantly outperform Shor codes, of the same length and minimum distance. Second, we consider the fault-tolerant preparation of Q_1 code states. We give a recursive procedure to prepare a Q_1 code state, based on two-qubit Pauli measurements only. The procedure is not by itself fault-tolerant, however, the measurement operations therein provide redundant classical bits, which can be advantageously used for error detection. Fault tolerance is then achieved by combining the proposed recursive procedure with an error detection method. Finally, we consider the fault-tolerant error correction of Q_1 codes. We use Steane's error correction technique, which incorporates the proposed fault-tolerant code state preparation procedure. We provide numerical estimates of the logical error rates for Q_1 and Shor codes of length 16 and 64 qubits, assuming a circuit-level depolarizing noise model. Remarkably, the Q_1 code of length 64 qubits achieves a pseudothreshold value slightly below 1%, demonstrating the potential of polar codes for fault-tolerant quantum computing.

1 Introduction

Quantum computers exploit counterintuitive properties of qubits, such as quantum entanglement and quantum superposition, to gain computational advantages. For unleashing their full computational power, a critical task is to protect the quantum computation from the inherent quantum noise. Thus, large scale quantum computers are expected to use quantum error correcting (QEC) codes to provide resilience against noise [1].

A quantum code encodes one or more logical qubits into many noisy physical qubits, so that the logical qubits are more robust against noise than the physical qubits. However, an efficient quantum code alone does not provide the ability to do fault-tolerant quantum computation (FTQC). To avoid the uncontrolled propagation of error, it must be complemented with several *fault-tolerant* procedures [2], aimed at (i) preparing logical code states, (ii) operating on logical states, and (iii) performing error correction.

For quantum stabilizer codes [3] correcting Pauli errors, fault-tolerant error correction relies on the use of an ancilla system, which is interacted in a specific and fault-tolerant way with the

encoded logical state (without disturbing the encoded quantum information), and then measured. Different fault-tolerant error correction methods exist, as for instance those proposed by Shor [4, 5], Steane [6, 7], and Knill [8]. The classical information outputted by the measurement operation, usually referred to as *error syndrome*¹, is then processed by a classical decoding algorithm, which determines the Pauli error that has happened, so that the quantum system can be returned to the correct logical state.

Currently, topological quantum codes [9–13], and more generally quantum low-density parity-check (LDPC) codes [14–19] are promising candidates for FTQC. These codes have low-weight stabilizer generators, which allows simple fault-tolerant syndrome extraction and logical state preparation. However, decoding quantum LDPC codes is in general a difficult problem. Indeed, while the fundamental motivation behind classical LDPC codes is to enable low-complexity message-passing decoding, such a decoding approach is unfortunately ruled out in the quantum case by the fact that quantum LDPC codes are highly degenerate [20]. Thus, decoding solutions are usually devised on a case-by-case basis. This is currently a very active area of research, where a lot of efforts are being dedicated to improving and designing new decoders for quantum LDPC (including topological) codes, see for instance [21–29] and references therein. It is worth noticing that a low-complexity decoding² algorithm is a key ingredient of FTQC. As noticed in [30], decoding must be faster than the syndrome extraction rate, since otherwise the latency overhead becomes exponential in the number of non-Clifford gates, hindering any quantum advantage.

In this paper, we explore an alternative approach to FTQC, relying on quantum polar codes. Introduced first in 2009 for classical systems [31], and then generalized to the quantum case [32–35], polar codes arguably represent one of the most important advances in coding theory of the past decade. They achieve the coherent information (one-shot capacity) of any quantum channel, and come equipped with an efficient decoding algorithm, known as successive cancellation (SC), whose complexity scales log-linearly with the code length. Yet, despite their excellent error correction properties, polar codes have been hardly explored for quantum computing, except the work in [36] on magic state distillation using punctured polar codes. However, no method for fault-tolerant preparation of quantum polar codes is known to date.

We consider quantum polar codes of Calderbank-Shor-Steane (CSS) type [32], encoding one logical qubit, which we refer to as \mathcal{Q}_1 codes. We note that the case of CSS codes encoding one logical qubit is of practical interest to FTQC, since it allows the simplest form of fault-tolerant logical controlled-NOT (CNOT) gate, by applying the physical CNOT gate transversely, across the physical qubits in the two codeblocks encoding the control and target logical qubits.

The standard (but non fault-tolerant) encoding procedure of \mathcal{Q}_1 codes is simple. Let Q_N denote the *quantum polar transform* on N qubits, where $N = 2^n$ ($n > 0$) is a power of two. We recall that Q_N is defined based on the recursive application of the quantum CNOT gate, transversely, on subblocks of 2^k qubits, for $k = 0, \dots, n - 1$ [31, 32]. To encode one logical qubit

¹Strictly speaking, the classical information retrieved by using either Steane or Knill error correction method is not an error syndrome, but an error corrupted version of a random codeword (of course, if needed, one may classically compute the corresponding syndrome).

²Here and in the sequel, by “decoding” (algorithm) we mean the classical algorithm that processes the extracted error syndrome to determine the error that has happened.

into N physical qubits, say $|q_1\rangle, \dots, |q_N\rangle$, we first select an *information index* $i \in \{1, \dots, N\}$. Qubit $|q_i\rangle$ is prepared in the quantum state we want to encode, while qubits $|q_1\rangle, \dots, |q_{i-1}\rangle$ are *frozen* in the Z -basis (that is, they are prepared as either $|0\rangle$ or $|1\rangle$) and qubits $|q_{i+1}\rangle, \dots, |q_N\rangle$ are frozen in the X -basis (that is, they are prepared as either $|+\rangle$ or $|-\rangle$). Then, we apply the quantum polar transform Q_N on the N -qubit product state $|q_1\rangle \otimes \dots \otimes |q_N\rangle$. The error correction capability of the Q_1 code (assuming the encoded state is subject to quantum noise) depends on the choice of the information index i . Assuming a noise model described by a quantum channel W with qubit input, acting independently on each of the N qubits, the quantum polar transform Q_N is known to induce a so-called *channel polarization* phenomenon, in both Z and X bases, based on which one may determine the information index i yielding the best error correction capability. We mention that the information index i may depend on the specific quantum channel W , thus allowing the optimization of the Q_1 code to the specific noise model.

The main contributions of our paper are as follows.

First, we show that a subfamily of Q_1 codes is equivalent to the well-known family of Shor codes [37,38]. Precisely, if the information position i is a power of two, that is, $i = 2^k, 0 \leq k \leq n$, the corresponding Q_1 code is a Shor code. We refer to these codes as Shor- Q_1 codes³, or simply Shor codes, when no confusion is possible. Hence, Q_1 codes can be seen as a generalization of the Shor's construction, providing significantly better error correction capability. We use the density evolution technique to estimate the performance of Q_1 codes under the SC decoding, for the quantum erasure and the quantum depolarizing channels. We show that the best Q_1 code significantly outperforms the best Shor- Q_1 code, even if both codes have the same minimum distance (and of course, the same code length N). This is owing to the SC decoding, which is able to decode beyond the minimum distance of the code, and to effectively exploit the choice of the information index based on the channel polarization property (or, to a certain extent, the degree of freedom provided by the full flexibility on the choice of the information index).

Second, we consider the fault-tolerant preparation of Q_1 code states. It is easily seen that the encoding procedure described above is not fault-tolerant, in the sense that an error due to a failure in one of the CNOT gates (composing Q_N) may propagate to many qubits through the CNOT gates that are applied after. Measuring the stabilizer generators using the standard “phase kickback trick” [2], similar to the case of quantum LDPC codes⁴, is also not fault-tolerant, due to the high weight of the generators. Hence, we propose a method to prepare a Q_1 code state, based on two-qubit Pauli measurements only. The proposed method consists of a recursive procedure, that prepares a code state of length 2^k by performing transversal Pauli $Z \otimes Z$ or Pauli $X \otimes X$ measurements, on two code states of length 2^{k-1} , for $k = 1, \dots, n$ (and where a code state of length 2^0 is simply a qubit initialized in the Z basis). This procedure is not by itself fault-tolerant, however, the measurement operations therein provide redundant

³In general, a Shor code is of length $N = K_1 K_2$, with $K_1, K_2 > 0$, where qubits are arranged on a two-dimensional square lattice of size $K_1 \times K_2$. Shor- Q_1 codes have length $N = 2^n$, with $K_1 = 2^k$ and $K_2 = 2^{n-k}$, for some $k = 0, \dots, n$.

⁴The error syndrome may be extracted by measuring the stabilizer generators, where one ancilla qubit is used for each generator, which interacts with all the data qubits acted on by the generator (phase kickback trick). While this procedure may propagate errors and is not in general fault-tolerant, it is still convenient for quantum LDPC codes, owing to their low-weight generators, which limit the propagation of errors.

classical bits, which can be advantageously used for error detection. Hence, to achieve fault tolerance, the proposed procedure is complemented by an error detection method.

Finally, we consider the fault-tolerant error correction of \mathcal{Q}_1 codes, using Steane's error correction technique. Assuming a block of N data (physical) qubits, encoding an arbitrary logical state, Steane's error correction technique works as follows. First, a block of N ancilla qubits is prepared in some logical state of the \mathcal{Q}_1 code (either logical $|0\rangle$, to correct Z errors, or logical $|+\rangle$, to correct X errors). Then a transverse CNOT gate is applied on ancilla and data qubits, in such a way that errors on the data qubits are copied to the ancilla qubits, while ancilla and data systems remain separated. Measuring the ancilla qubits outputs an error-corrupted version of some (random) codeword of a classical polar code (in either Z or X basis). Finally, classical SC decoding is applied to determine the error, and then the corrective operation is applied to the data qubits. Hence, the error correction procedure essentially reduces to the preparation of a logical \mathcal{Q}_1 code state, for which we use the proposed fault-tolerant preparation procedure. We provide numerical estimates of the logical error rates using Steane's error correction technique, assuming a circuit-level depolarizing noise model, for \mathcal{Q}_1 and Shor- \mathcal{Q}_1 codes of length $N = 16$ and $N = 64$ qubits.

The paper is organized as follows. In Section 2, we present the relevant background on classical and CSS quantum polar codes, and detail the Steane fault-tolerant error-correction procedure applied to CSS quantum polar codes. In Section 3, we introduce \mathcal{Q}_1 codes, discuss their construction (*i.e.*, choice of the information position), and provide a comparison between the error-correction performance of \mathcal{Q}_1 and Shor- \mathcal{Q}_1 codes, for the quantum depolarizing and quantum erasure channels, assuming ideal (error-free) syndrome extraction. In Section 4, we present our recursive preparation procedure of \mathcal{Q}_1 code states, based two-qubit Pauli measurements. We first describe our preparation procedure in the error-free case (and show that it does indeed prepare the expected \mathcal{Q}_1 code state), then, in the presence of errors, we show that it can be made fault-tolerant by incorporating an error detection mechanism. In Section 5, we present our numerical results on the logical error rates of \mathcal{Q}_1 and Shor- \mathcal{Q}_1 codes, using Steane's error correction procedure. Finally, Section 6 concludes the paper.

2 Preliminaries

Here, we first describe classical polar codes [31] and then explain how quantum polar codes of CSS type [32] are constructed, using classical polar codes.

Notation. The following notation will be used throughout the paper.

- (1) Unless otherwise stated, we shall assume column vectors and denote them by bold letters such as $\mathbf{u}, \mathbf{v}, \mathbf{x}, \mathbf{z}, \dots$. For a vector $\mathbf{u} \in \{0, 1\}^N$, we write $\mathbf{u} = (u_1, \dots, u_N)$, where $u_1, \dots, u_N \in \{0, 1\}$. We use $\mathbf{0}$ and $\mathbf{1}$ to denote the all-zero and all-one vectors, respectively.
- (2) For $\mathbf{u} \in \{0, 1\}^N$, we define $\text{supp}(\mathbf{u}) := \{i \in \{1, \dots, N\} \mid u_i = 1\}$ and $\text{wt}(\mathbf{u}) := |\text{supp}(\mathbf{u})|$. Further, for a subset $\mathcal{A} \subseteq \{1, \dots, N\}$, we denote $\mathbf{u}|_{\mathcal{A}}$ to be the part of \mathbf{u} corresponding to the indices in \mathcal{A} .

(3) We often denote Pauli X basis states as $|\bar{0}\rangle := |+\rangle$ and $|\bar{1}\rangle := |-\rangle$.

Further, for $\mathbf{u} \in \{0, 1\}^N$, we define

$$|\mathbf{u}\rangle := |u_1\rangle \otimes \cdots \otimes |u_n\rangle, \quad (1)$$

$$|\bar{\mathbf{u}}\rangle := |\bar{u}_1\rangle \otimes \cdots \otimes |\bar{u}_n\rangle, \quad (2)$$

(4) For a Pauli unitary $P \in \{X, Y, Z\}$ and $\mathbf{u} \in \{0, 1\}^N$, we define

$$P^{\mathbf{u}} := P^{u_1} \otimes \cdots \otimes P^{u_n}. \quad (3)$$

2.1 Classical Polar Codes

2.1.1 Encoding

The encoding of classical polar codes is done by applying the reversible XOR gate recursively on an N bit input $\mathbf{u} = (u_1, \dots, u_N) \in \{0, 1\}^N$, where $N = 2^n$, with $n > 0$ (see Fig. 1). For a set of positions $\mathcal{F} \subseteq \{1, \dots, N\}$, the corresponding component $\mathbf{u}|_{\mathcal{F}} \in \{0, 1\}^{|\mathcal{F}|}$ of the input vector \mathbf{u} is frozen. We may take $\mathbf{u}|_{\mathcal{F}}$ to be any vector in $\{0, 1\}^{|\mathcal{F}|}$, but it should be known to both the encoder and decoder. The set \mathcal{F} is called the *frozen set*. The remaining positions $\mathcal{I} := \{1, \dots, N\} \setminus \mathcal{F}$ are used to encode information bits. The set \mathcal{I} is called the *information set*.

In the following, we denote by $\mathcal{P}(N, \mathcal{F}, \mathbf{u}|_{\mathcal{F}})$, the classical polar code of length N , frozen positions \mathcal{F} , and frozen vector $\mathbf{u}|_{\mathcal{F}} \in \{0, 1\}^{|\mathcal{F}|}$.

The action of the $\text{XOR}_{2 \rightarrow 1}$ gate on input $\mathbf{u} = (u_1, u_2) \in \{0, 1\}^2$ gives $\mathbf{x} = (u_1 \oplus u_2, u_2)$. In matrix form, we may write $\mathbf{x} = P_2 \mathbf{u}$, where

$$P_2 = \begin{bmatrix} 1 & 1 \\ 0 & 1 \end{bmatrix} \quad (4)$$

The classical polar transform, that is, the recursive application of $\text{XOR}_{2 \rightarrow 1}$ on $N = 2^n$ qubits, is thus given by the matrix

$$P_N = P_2^{\otimes n}. \quad (5)$$

For any value of the information bits $\mathbf{u}_{\mathcal{I}} \in \{0, 1\}^{|\mathcal{I}|}$, $\mathbf{x} = P_N(\mathbf{u}|_{\mathcal{F}}, \mathbf{u}|_{\mathcal{I}}) \in \{0, 1\}^N$ is a codeword of the polar code $\mathcal{P}(N, \mathcal{F}, \mathbf{u}|_{\mathcal{F}})$. If $\mathbf{u}|_{\mathcal{F}}$ is the all zero vector, the polar code $\mathcal{P}(N, \mathcal{F}, \mathbf{u}|_{\mathcal{F}})$ is generated by the columns of P_N corresponding to the information set \mathcal{I} .

2.1.2 Construction

The *construction* of a classical polar code refers to the choice of the information set \mathcal{I} (or, equivalently, the frozen set \mathcal{F}). This is done in a *channel specific way* as follows.

Consider a discrete, memoryless, classical channel $W(y | x)$, with binary input $x \in \{0, 1\}$, and output $y \in \mathcal{Y}$. For $\mathbf{u} \in \{0, 1\}^N$, let $\mathbf{x} = P_N(\mathbf{u}) \in \{0, 1\}^N$ (note that here \mathcal{F} and \mathcal{I} need not be defined) and $\mathbf{y} \in \mathcal{Y}^N$ be the output corresponding to N uses of the W channel, with inputs x_1, \dots, x_N . For $i = 1, \dots, N$, let $W^{(i)}(\mathbf{y}, \mathbf{u}_{1:i-1} | u_i)$ denote the so-called *virtual channel*, with input $u_i \in \{0, 1\}$ and output $(\mathbf{y}, \mathbf{u}_{1:i-1}) \in \mathcal{Y} \times \{0, 1\}^{i-1}$, where $\mathbf{u}_{1:i-1} := (u_1, \dots, u_{i-1})$.

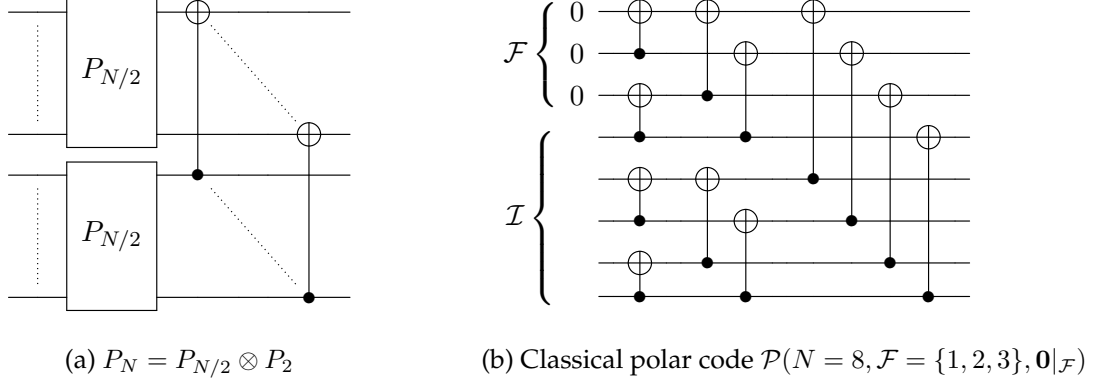


Fig. 1: (a) Polar transform recursion: P_N in terms of $P_{N/2}$. (b) Example of a classical polar code encoding $|\mathcal{I}| = 5$ bits into $N = 2^3$ bits, with frozen set $\mathcal{F} = \{1, 2, 3\}$, and frozen vector $u_{\mathcal{F}} = (0, 0, 0)$. Here, the set \mathcal{F} (thus, \mathcal{I}) is chosen only for the purpose and the simplicity of the illustration. In general, it needs not consist of consecutive positions.

Informally, the *channel polarization theorem* [31] states that, for sufficiently large N , almost all the virtual channels become arbitrarily close to either the noiseless (perfect) channel or to the completely noisy (useless) channel. The *closeness* to the either perfect or useless channel can be expressed in terms of different parameters, such as the mutual information $I(W^{(i)})$, the Bhattacharyya parameter $Z(W^{(i)})$, or the error probability $P_e(W^{(i)})$, which can be computed analytically for some channels (e.g., binary erasure channels), or estimated numerically through *density evolution*, for more general channels [39]. Once one of these parameters is computed for all the virtual channels, they are sorted from the most reliable (closest to the perfect channel) to the least reliable (closest to the useless channel) one.

For a polar code encoding K information bits, the information set \mathcal{I} consists of the indexes corresponding to the K most reliable virtual channels (equivalently, the $N - K$ least reliable virtual channels are frozen). The usefulness of this construction will become apparent in relation to the successive cancellation decoding, discussed in the next section.

2.1.3 Decoding

Classical polar codes come equipped with an efficient successive cancellation (SC) decoding algorithm. SC decoding takes advantage of the polar code construction, by estimating inputs u_1, \dots, u_N sequentially. For $i = 1, \dots, N$, SC decoding outputs the *maximum a posteriori estimate* \hat{u}_i of u_i , conditional on the observed output \mathbf{y} and previous estimates $\hat{\mathbf{u}}_{1:i-1} = (\hat{u}_1, \dots, \hat{u}_{i-1})$. Precisely, we have⁵

$$\hat{u}_i := \begin{cases} u_i, & \text{if } i \in \mathcal{F} \\ \arg \max_{u \in \{0,1\}} W^{(i)}(\mathbf{y}, \hat{\mathbf{u}}_{1:i-1} | u), & \text{if } i \in \mathcal{I} \end{cases} \quad (6)$$

If the information set contains indexes of *good virtual channels* (close to the perfect channel), the maximum a posteriori estimate \hat{u}_i is equal to the input u_i with high probability. This does not happen for *bad virtual channels* (close to the useless channel), which must then be frozen, so that

⁵Here, we use the same notation for a channel $W^{(i)}$ and the corresponding conditional probabilities between channel output and input.

the corresponding inputs are known to both the encoder and decoder. It is worth noticing that the maximum a posteriori decoding of the virtual channels can be performed in an efficient way, by using a message passing algorithm that takes advantage of the recursive structure of the polar code [31]. Overall, the complexity of the SC decoding scales as $O(N \log(N))$.

Finally, we note that Polar codes under SC decoding are known to *achieve the channel capacity* [31]. This means that for sufficiently large N , it is possible to choose an information set of size $|\mathcal{I}|$ arbitrary close of $NI(W)$, where $I(W)$ is the channel's mutual information, while ensuring an arbitrary small error probability under SC decoding.

2.2 CSS Quantum Polar Codes

2.2.1 Encoding

The encoding of CSS quantum polar codes is done by applying the quantum CNOT gate recursively on an N -qubit quantum state $|\psi\rangle_{\mathcal{S}}$, where $\mathcal{S} := \{1, \dots, N\}$ denotes an N -qubit quantum system (Fig. 2).

The quantum CNOT gate induces the reversible XOR gate in the Pauli Z and Pauli X bases. Precisely, $\text{CNOT}_{2 \rightarrow 1}$ acts as $\text{XOR}_{2 \rightarrow 1}$ in the Pauli Z basis, while it acts as $\text{XOR}_{1 \rightarrow 2}$ in the Pauli X basis. Let Q_N be the quantum polar transform, that is, the unitary operator corresponding to the recursive action of the CNOT gates on N qubits. Hence, it follows that Q_N acts as the classical polar transform P_N in the Pauli Z basis, while it acts as the reverse classical polar transform (*i.e.*, with inverted target and control bits) in the Pauli X basis.

It can be seen that the reversed classical polar transform is described by P_N^\top , where P_N^\top is the transpose of P_N [32]. Therefore, we have the following, for $\mathbf{u} \in \{0, 1\}^N$,

$$Q_N|\mathbf{u}\rangle = |P_N\mathbf{u}\rangle, \quad (7)$$

$$Q_N|\overline{\mathbf{u}}\rangle = |\overline{P_N^\top\mathbf{u}}\rangle. \quad (8)$$

For CSS quantum polar codes, the quantum information is encoded as follows (Fig. 2). For a subset of positions $\mathcal{Z} \subseteq \mathcal{S}$, the input quantum state is frozen to a known Pauli Z basis state $|\mathbf{u}\rangle_{\mathcal{Z}}$, where $\mathbf{u} \in \{0, 1\}^{|\mathcal{Z}|}$, and for another subset $\mathcal{X} \subseteq \mathcal{S}$, with $\mathcal{Z} \cap \mathcal{X} = \emptyset$, it is frozen to a known Pauli X basis state $|\overline{\mathbf{v}}\rangle_{\mathcal{X}}$, where $\mathbf{v} \in \{0, 1\}^{|\mathcal{X}|}$.

The remaining subset $\mathcal{I} := \mathcal{S} \setminus (\mathcal{X} \cup \mathcal{Z})$ is used to encode a quantum state $|\phi\rangle_{\mathcal{I}}$. Hence, the quantum state $|\mathbf{u}\rangle_{\mathcal{Z}} \otimes |\phi\rangle_{\mathcal{I}} \otimes |\overline{\mathbf{v}}\rangle_{\mathcal{X}}$ is given as input to the polar transform Q_N . The encoded logical code state, denoted by $|\tilde{\phi}\rangle_{\mathcal{S}}$, is given by

$$|\tilde{\phi}\rangle_{\mathcal{S}} = Q_N(|\mathbf{u}\rangle_{\mathcal{Z}} \otimes |\phi\rangle_{\mathcal{I}} \otimes |\overline{\mathbf{v}}\rangle_{\mathcal{X}}). \quad (9)$$

In the following, we denote by $\mathcal{Q}(N, \mathcal{Z}, \mathcal{X}, |\mathbf{u}\rangle_{\mathcal{Z}}, |\overline{\mathbf{v}}\rangle_{\mathcal{X}})$, the quantum polar code on N qubits, with frozen sets \mathcal{Z} and \mathcal{X} , corresponding to the Pauli Z and Pauli X bases, respectively, and with corresponding frozen quantum states $|\mathbf{u}\rangle_{\mathcal{Z}}$ and $|\overline{\mathbf{v}}\rangle_{\mathcal{X}}$. It induces two classical polar codes, one in Z basis, with frozen set \mathcal{Z} , and one in X basis, with frozen set \mathcal{X} , where the latter is defined by a reversed polar transform, as illustrated in Fig. 3. Let π denote the *reverse order permutation* of $\mathcal{S} = \{1, \dots, N\}$, defined by $\pi(i) = N + 1 - i$. Then, the classical polar code

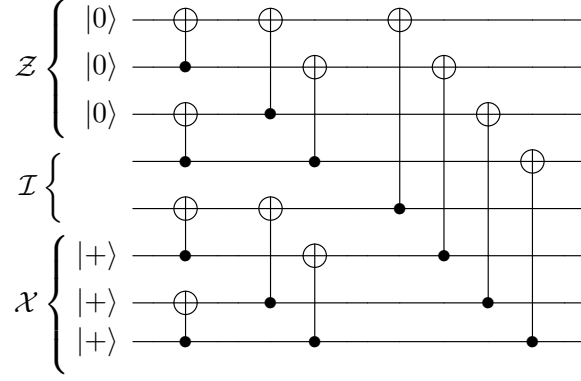


Fig. 2: The quantum polar code $Q(N, \mathcal{Z}, \mathcal{X}, |\mathbf{u}\rangle_{\mathcal{Z}}, |\bar{\mathbf{v}}\rangle_{\mathcal{X}})$, with $N = 2^3$, frozen sets $\mathcal{Z} = \{1, 2, 3\}$, $\mathcal{X} = \{6, 7, 8\}$, and frozen states $|\mathbf{u}\rangle_{\mathcal{Z}} = |0, 0, 0\rangle$, and $|\bar{\mathbf{v}}\rangle_{\mathcal{X}} = |+, +, +\rangle$. Here, the sets \mathcal{Z} and \mathcal{X} (thus, \mathcal{I}) are chosen only for the purpose and the simplicity of the illustration. In general, they need not consist of consecutive positions.

induced in the Z basis is $\mathcal{P}(N, \mathcal{Z}, \mathbf{u})$, while the classical polar code induced in the X basis is $\mathcal{P}(N, \pi(\mathcal{X}), \pi(\mathbf{v}))$, where the vector $\pi(\mathbf{v})$ is defined by permuting the entries of \mathbf{v} according to π , that is, $\pi(\mathbf{v})_i := v_{\pi(i)}$, $\forall i \in \mathcal{X}$.

The X and Z type stabilizer generators of $Q(N, \mathcal{Z}, \mathcal{X}, |\mathbf{u}\rangle_{\mathcal{Z}}, |\bar{\mathbf{v}}\rangle_{\mathcal{X}})$ are given by the lemma below.

Lemma 1. Let $\mathbf{e}_i \in \{0, 1\}^N$ be the binary vector, with 0 everywhere except 1 at the i -th position. Then, the stabilizer group of $Q(N, \mathcal{Z}, \mathcal{X}, |\mathbf{u}\rangle_{\mathcal{Z}}, |\bar{\mathbf{v}}\rangle_{\mathcal{X}})$ is generated by the following X and Z type operators

$$(-1)^{v_i} X^{P_N \mathbf{e}_i}, \forall i \in \mathcal{X}. \quad (10)$$

$$(-1)^{u_i} Z^{P_N^\top \mathbf{e}_i}, \forall i \in \mathcal{Z}. \quad (11)$$

Proof. Note that the input of the polar transform in (9), that is, the quantum state $|\mathbf{u}\rangle_{\mathcal{Z}} \otimes |\phi\rangle_{\mathcal{I}} \otimes |\bar{\mathbf{v}}\rangle_{\mathcal{X}}$, is stabilized by the following Pauli operators

$$(-1)^{v_i} X^{\mathbf{e}_i}, \forall i \in \mathcal{X}, \quad (12)$$

$$(-1)^{u_i} Z^{\mathbf{e}_i}, \forall i \in \mathcal{Z}. \quad (13)$$

Therefore, the encoded quantum state $|\tilde{\phi}\rangle_{\mathcal{S}}$ is stabilized by the following Pauli operators,

$$(-1)^{v_i} Q_N X^{\mathbf{e}_i} Q_N, \forall i \in \mathcal{X}, \quad (14)$$

$$(-1)^{u_i} Q_N Z^{\mathbf{e}_i} Q_N, \forall i \in \mathcal{Z}. \quad (15)$$

The operators in (14)-(15) are a generating set of the stabilizer group of $Q(N, \mathcal{Z}, \mathcal{X}, |\mathbf{u}\rangle_{\mathcal{Z}}, |\bar{\mathbf{v}}\rangle_{\mathcal{X}})$. These generators can be written in terms of classical polar transforms P_N and P_N^\top as follows.

We first consider the case of two qubits, and observe that the sandwiching actions of the CNOT gate on Pauli operators gives, for $\mathbf{u} \in \{0, 1\}^2$,

$$\text{CNOT}_{2 \rightarrow 1} X^{\mathbf{u}} \text{CNOT}_{2 \rightarrow 1} = X^{P_2 \mathbf{u}}, \quad (16)$$

$$\text{CNOT}_{2 \rightarrow 1} Z^{\mathbf{u}} \text{CNOT}_{2 \rightarrow 1} = Z^{P_2^\top \mathbf{u}}. \quad (17)$$

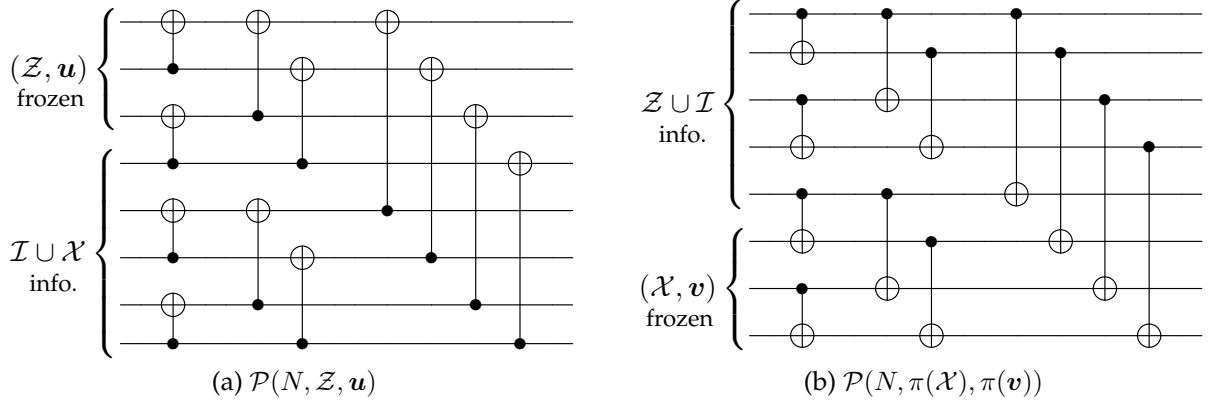


Fig. 3: Classical polar codes in (a) Z basis, and (b) X basis, induced by the CSS quantum polar code in Fig. 2. The permutation π in (b) is the reverse order permutation. (Note that in this example the two codes are actually the same.)

Using (16)-(17) and (5), the sandwiching action of Q_N is described by the classical polar transforms P_N and P_N^\top , respectively, on X and Z type operators. Hence, the stabilizer generators from (14)-(15) can be written as given in (10)-(11) \square

Note, from (10), that the indicator vector of X -type generators are given by the columns of P_N , corresponding to the set \mathcal{X} . Further, from (11), the indicator vectors of the Z -type generators are given by the columns of P_N^\top (*i.e.*, the rows of P_N), corresponding to the set \mathcal{Z} .

Similarly to Lemma 1, logical Pauli operators can be determined by passing X and Z operators through the polar transform, as shown in the lemma below.

Lemma 2. Let \tilde{X}_i and \tilde{Z}_i be the logical X and Z operators, corresponding to the encoded qubit at the position $i \in \mathcal{I}$. Then,

$$\tilde{X}_i = X^{P_N \mathbf{e}_i}, \quad (18)$$

$$\tilde{Z}_i = Z^{P_N^\top \mathbf{e}_i}. \quad (19)$$

2.2.2 Construction

The *construction* of a CSS quantum polar code refers to determining the frozen sets \mathcal{Z} and \mathcal{X} (thus, the information set \mathcal{I}), which exploits the classical polarization in Z and X bases, respectively [32]. We shall assume a Pauli channel \mathcal{W} , with qubit input, given by

$$\mathcal{W}(\rho) = p_I \rho + p_X X \rho X + p_Y Y \rho Y + p_Z Z \rho Z, \quad (20)$$

where ρ denotes the density matrix of the qubit (mixed) state, and $p_I, p_X, p_Y, p_Z \in [0, 1]$ are probability values, summing to 1.

In Z basis, only X errors matter. Thus, the channel induced in the Z -basis, denoted W_Z , captures the effect of X -type errors on the quantum state, and is given by

$$W_Z(|u\rangle\langle u|) = (p_I + p_Z)|u\rangle\langle u| + (p_X + p_Y)X|u\rangle\langle u|X, \quad u \in \{0, 1\}. \quad (21)$$

Hence, W_Z is a classical binary symmetric channel (BSC), with error probability $p_X + p_Y$.

Similarly, the X -basis induced channel, denoted W_X , captures the effect of Z -type errors on the quantum state, and is given by

$$W_X(|\bar{u}\rangle\langle\bar{u}|) = (p_I + p_X)|\bar{u}\rangle\langle\bar{u}| + (p_Z + p_Y)Z|\bar{u}\rangle\langle\bar{u}|Z, \quad u \in \{0, 1\}. \quad (22)$$

Hence, W_X is a classical BSC, with error probability $p_X + p_Y$.

To construct the CSS quantum polar code, we exploit the classical polarization of W_Z and W_X channels. Note that this construction *ignores the correlations* between X and Z (we will explain how these correlations can be captured a little later, below). The frozen set \mathcal{Z} is determined by the classical polarization of the W_Z channel, under the classical polar transform P_N , while the frozen set \mathcal{X} is determined by the classical polarization of the W_X , under the reversed classical polar transform P_N^\top . The remaining information set \mathcal{I} corresponds to virtual channels that are *good* (Section 2.1.3) in both Z and X bases. The frozen set \mathcal{Z} corresponds to virtual channels that are *bad* in Z basis. These channels may be either bad or good in X basis, it does not matter, since we need not decode Z errors on corresponding inputs (such errors correspond to Z -type generators, thus they act trivially on the code space). Similarly, the frozen set \mathcal{X} corresponds to virtual channels that are bad in X basis, and which may be either bad or good in Z basis⁶.

To *capture the correlations* between X and Z errors, one of the two channels, say W_X , has to be *extended* [32]. The extended channel, denoted by $W_{X'}$, is thus defined by the conditional probability of a Z error, given the X error. Precisely,

$$\begin{aligned} W_{X'}(|\bar{u}\rangle\langle\bar{u}|) = & (p_I + p_Z)|0\rangle\langle 0|_X \otimes \left(\frac{p_I}{p_I + p_Z}|\bar{u}\rangle\langle\bar{u}| + \frac{p_Z}{p_I + p_Z}Z|\bar{u}\rangle\langle\bar{u}|Z \right) + \\ & (p_X + p_Y)|1\rangle\langle 1|_X \otimes \left(\frac{p_X}{p_X + p_Y}|\bar{u}\rangle\langle\bar{u}| + \frac{p_Y}{p_X + p_Y}Z|\bar{u}\rangle\langle\bar{u}|Z \right) \end{aligned} \quad (23)$$

where $\{|0\rangle_X, |1\rangle_X\}$ is an orthogonal basis of an auxiliary system, indicating whether an X error happened or not. Put differently, $W_{X'}$ is a classical mixture of two BSCs, the first with error probability $p_Z/(p_I + p_Z)$ (when no X error happened), and the second with error probability $p_Y/(p_X + p_Y)$ (when an X error happened).

The construction of the CSS quantum polar code, taking into account the correlations between X and Z errors, is done in the same way as above, while replacing the W_X channel by its extended version $W_{X'}$.

2.2.3 Steane Error Correction

We describe here the Steane error correction procedure [6, 7] (see also [2, Section 4.4]), applied to CSS quantum polar codes. Throughout this section, we consider an encoded state $|\tilde{\phi}\rangle_S = Q_N(|\mathbf{u}\rangle_{\mathcal{Z}} \otimes |\phi\rangle_{\mathcal{I}} \otimes |\bar{\mathbf{v}}\rangle_{\mathcal{X}})$ of the quantum polar code $\mathcal{Q}(N, \mathcal{Z}, \mathcal{X}, |\mathbf{u}\rangle_{\mathcal{Z}}, |\bar{\mathbf{v}}\rangle_{\mathcal{X}})$, that we want to protect against Pauli errors.

Steane's error correction procedure consists of the following steps.

⁶Precisely, positions in \mathcal{X} that do not impact the decoding of subsequent positions in \mathcal{I} (if any) may correspond to bad virtual channels in Z basis. For instance, this may be the case for some positions in \mathcal{X} that come after the last position in \mathcal{I} , *i.e.*, some $j \in \mathcal{X}$, such that $i < j, \forall i \in \mathcal{I}$. See also Fig. 3a.

- (1) An ancilla system \mathcal{S}' is prepared in either the logical all- $|+\rangle$ state or the logical all- $|0\rangle$ state of $\mathcal{Q}(N, \mathcal{Z}, \mathcal{X}, |\mathbf{u}\rangle_{\mathcal{Z}}, |\mathbf{v}\rangle_{\mathcal{X}})$. The former state is prepared for X -error correction, while the latter of Z -error correction.
- (2) A transverse CNOT gate is applied between \mathcal{S} (original) and \mathcal{S}' (ancilla) systems, in such a way that either the X or the Z errors on \mathcal{S} are copied to \mathcal{S}' , while the two systems remain separated.
- (3) The ancilla system is measured, outputting a random codeword of a classical polar code (in either Z or X basis), corrupted by the error that has been copied to \mathcal{S}' .
- (4) A classical SC decoding is applied to determine the error (possibly, the corresponding corrective operation is applied on the \mathcal{S} system).

It is easily seen that steps (2) and (3) are fault-tolerant, as they consist only of transverse gates and single qubit measurements. The fault-tolerant preparation of the ancilla system \mathcal{S}' (step (1)) will make the object of Section 4 (for the particular case of \mathcal{Q}_1 codes, introduced in Section 3).

By a slight abuse of language, we shall refer to steps (1)-(3) above as *syndrome extraction*. In case of *ideal syndrome extraction*, steps (1)-(3) are assumed to be error free, and the error corrected at step (4) is the one preexisting on system \mathcal{S} , before the syndrome is extracted. In case of *noisy syndrome extraction*, steps (1)-(3) may generate additional errors on systems \mathcal{S} and \mathcal{S}' . We will analyze the impact of these errors, together with providing the details of Steane's error correction applied to either X or Z errors, on the two subsections below.

We will consider an ancilla system $\mathcal{S}' = \{1', \dots, N'\}$ and subsets $\mathcal{Z}', \mathcal{I}', \mathcal{X}' \subseteq \mathcal{S}'$. They are the counterparts of the subsets $\mathcal{Z}, \mathcal{I}, \mathcal{X} \subseteq \mathcal{S}$, in the sense that $i' \in \mathcal{Z}' \Leftrightarrow i \in \mathcal{Z}$, and similarly for \mathcal{I}' and \mathcal{X}' .

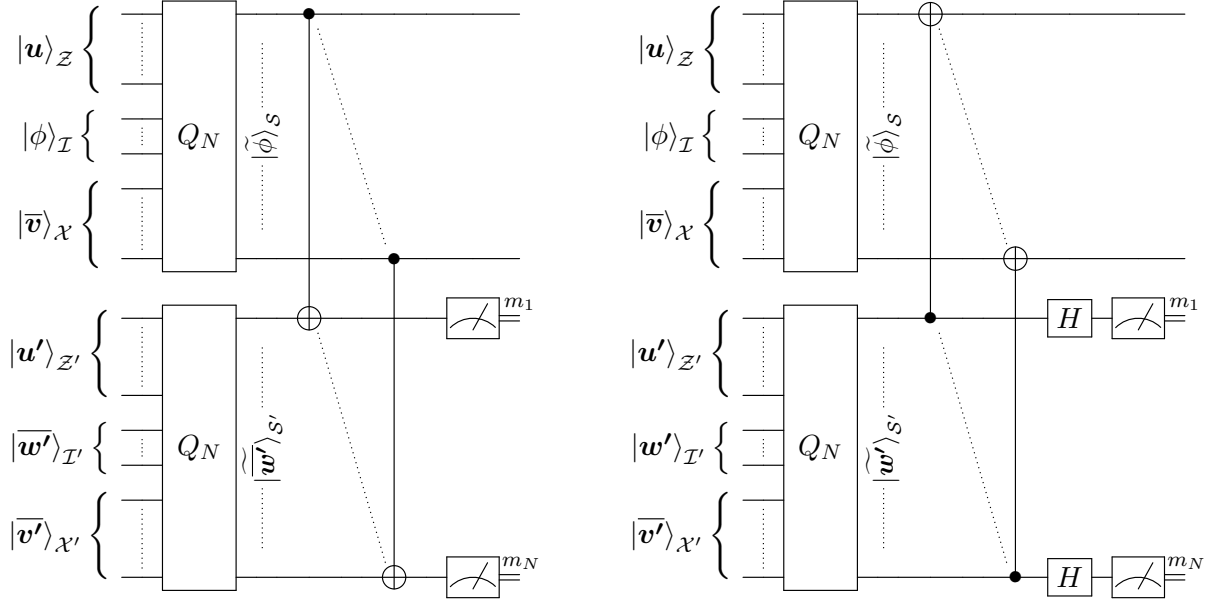
X -Error Correction. To extract the syndrome for X errors, the ancilla system $\mathcal{S}' = \mathcal{Z}' \cup \mathcal{I}' \cup \mathcal{X}'$ must be prepared in a logical X basis state. Usually, the ancilla state is taken to be the logical all- $|+\rangle$ state, obtained by encoding the all- $|+\rangle$ state on system \mathcal{I}' . Here, we consider a slightly more general logical X basis state, as follows,

$$|\widetilde{\mathbf{w}'}\rangle_{\mathcal{S}'} = Q_N(|\mathbf{u}'\rangle_{\mathcal{Z}'} \otimes |\overline{\mathbf{w}'}\rangle_{\mathcal{I}'} \otimes |\overline{\mathbf{v}'}\rangle_{\mathcal{X}'}), \quad (24)$$

where $\mathbf{u}', \mathbf{w}', \mathbf{v}'$ are known. Note that frozen values \mathbf{u}' and \mathbf{v}' may be different from frozen values \mathbf{u} and \mathbf{v} . The reason we consider the above logical state is that our preparation method for logical polar code states (given in Section 4 below) is measurement based, for which $\mathbf{u}', \mathbf{w}', \mathbf{v}'$ are determined based on random outcomes of measurements therein.

Steane's X -error syndrome extraction procedure is depicted in Fig. 4a. After preparing the state $|\widetilde{\mathbf{w}'}\rangle_{\mathcal{S}'}$ on system \mathcal{S}' , the qubitwise CNOT $_{\mathcal{S} \rightarrow \mathcal{S}'}$ gate is applied on corresponding qubits of systems \mathcal{S} and \mathcal{S}' . Then, each qubit in the ancilla system \mathcal{S}' is measured in the Pauli Z basis. We denote by $\mathbf{m} = (m_1, \dots, m_N)$ the classical outputs of these measurements.

The following lemma gives the state of the \mathcal{S} system, as well as the measurement result \mathbf{m} , after the syndrome extraction procedure. We consider errors e_X and e'_X that have happened



(a) X-error correction: X errors are copied from the original (top) to the ancilla (bottom) system, which is measured in Z basis.

(b) Z-error correction: Z errors are copied from the original (top) to the ancilla (bottom) system, which is measured in X basis.

Fig. 4: Steane's error correction method.

on systems \mathcal{S} and \mathcal{S}' , respectively. We assume that errors e_X and e'_X have happened before the qubitwise $\text{CNOT}_{\mathcal{S} \rightarrow \mathcal{S}'}$ gate is applied, while the qubitwise $\text{CNOT}_{\mathcal{S} \rightarrow \mathcal{S}'}$ gate, as well as the measurement operations, are error free. We refer to these errors as *preparation errors*. This assumption is made for simplicity only. Indeed, it is not too difficult to see that errors generated on the \mathcal{S}' system, by either the qubitwise $\text{CNOT}_{\mathcal{S} \rightarrow \mathcal{S}'}$ gate or the measurement operations, can actually be incorporated to the error e'_X . Errors generated by the qubitwise $\text{CNOT}_{\mathcal{S} \rightarrow \mathcal{S}'}$ gate on the \mathcal{S} system go undetected, but they may be corrected during the next round of error correction (see also Section 5.3).

Lemma 3. Let e_X and e'_X be preparation errors that have happened on systems \mathcal{S} and \mathcal{S}' , respectively. Then, after the Steane's X-error syndrome extraction, the state of the system \mathcal{S} is given by

$$X^{e_X} |\widetilde{Z^{w'}\phi}\rangle_{\mathcal{S}} = X^{e_X} Q_N(|u\rangle_{\mathcal{Z}} \otimes Z^{w'}|\phi\rangle_{\mathcal{I}} \otimes |\overline{v \oplus v'}\rangle_{\mathcal{X}}). \quad (25)$$

Further, the measurement outcome is a noisy codeword of the classical polar code $\mathcal{P}(N, \mathcal{Z}, \mathbf{u} \oplus \mathbf{u}')$, with frozen set \mathcal{Z} and frozen vector $\mathbf{u} \oplus \mathbf{u}'$, as follows,

$$\mathbf{m} = P_N(\mathbf{u} \oplus \mathbf{u}', \mathbf{a}', \mathbf{x}') \oplus \mathbf{e}_X \oplus \mathbf{e}'_X \in \{0, 1\}^N, \quad (26)$$

where $\mathbf{a}' \in \{0, 1\}^{|\mathcal{I}|}$ and $\mathbf{x}' \in \{0, 1\}^{|\mathcal{X}|}$ are random vectors.

Proof. Let $|\phi\rangle_{\mathcal{I}} = \sum_{\mathbf{a} \in \{0, 1\}^{|\mathcal{I}|}} \phi_{\mathbf{a}} |\mathbf{a}\rangle_{\mathcal{I}}$. Note also that $|\overline{v}\rangle_{\mathcal{X}} = \sum_{\mathbf{x} \in \{0, 1\}^{|\mathcal{X}|}} (-1)^{v \cdot \mathbf{x}} |\mathbf{x}\rangle_{\mathcal{X}}$ (up to a normalization factor, which will be omitted in the sequel). Then, the noisy logical state $X^{e_X} |\widetilde{\phi}\rangle_{\mathcal{S}}$ can be written as

$$X^{e_X} |\widetilde{\phi}\rangle_{\mathcal{S}} = X^{e_X} Q_N(|u\rangle_{\mathcal{Z}} \otimes |\phi\rangle_{\mathcal{I}} \otimes |\overline{v}\rangle_{\mathcal{X}}) = \sum_{\mathbf{a}, \mathbf{x}} \phi_{\mathbf{a}} (-1)^{v \cdot \mathbf{x}} |P_N(\mathbf{u}, \mathbf{a}, \mathbf{x}) \oplus \mathbf{e}_X\rangle. \quad (27)$$

Similarly, the noisy ancilla state can be written as

$$X^{e'_X} |\widetilde{\mathbf{w}'}\rangle_{S'} = X^{e'_X} Q_N(|\mathbf{u}'\rangle_{Z'} \otimes |\overline{\mathbf{w}'}\rangle_{I'} \otimes |\overline{\mathbf{v}'}\rangle_{X'}) = \sum_{\mathbf{a}', \mathbf{x}'} (-1)^{\mathbf{w}' \cdot \mathbf{a}' + \mathbf{v}' \cdot \mathbf{x}'} |P_N(\mathbf{u}', \mathbf{a}', \mathbf{x}') \oplus e'_X\rangle. \quad (28)$$

After the transverse CNOT $_{S \rightarrow S'}$ gate is applied, we get the following state on the bipartite SS' system,

$$|\theta\rangle_{SS'} := \text{CNOT}_{S \rightarrow S'} \left(X^{e_X} |\widetilde{\phi}\rangle_S \otimes X^{e'_X} |\widetilde{\mathbf{w}'}\rangle_{S'} \right) \quad (29)$$

$$= \sum_{\mathbf{a}, \mathbf{x}} \phi_{\mathbf{a}} (-1)^{\mathbf{v} \cdot \mathbf{x}} |P_N(\mathbf{u}, \mathbf{a}, \mathbf{x}) \oplus e_X\rangle \otimes \sum_{\mathbf{a}', \mathbf{x}'} (-1)^{\mathbf{w}' \cdot \mathbf{a}' + \mathbf{v}' \cdot \mathbf{x}'} |P_N(\mathbf{u} \oplus \mathbf{u}', \mathbf{a} \oplus \mathbf{a}', \mathbf{x} \oplus \mathbf{x}') \oplus e_X \oplus e'_X\rangle \quad (30)$$

$$= \sum_{\mathbf{a}, \mathbf{x}} \phi_{\mathbf{a}} (-1)^{\mathbf{w}' \cdot \mathbf{a} + (\mathbf{v} \oplus \mathbf{v}') \cdot \mathbf{x}} |P_N(\mathbf{u}, \mathbf{a}, \mathbf{x}) \oplus e_X\rangle \otimes \sum_{\mathbf{a}', \mathbf{x}'} (-1)^{\mathbf{w}' \cdot \mathbf{a}' + \mathbf{v}' \cdot \mathbf{x}'} |P_N(\mathbf{u} \oplus \mathbf{u}', \mathbf{a}', \mathbf{x}') \oplus e_X \oplus e'_X\rangle. \quad (31)$$

where for the last equality, we use variable changes $\mathbf{a}' \leftarrow \mathbf{a}' \oplus \mathbf{a}$, and $\mathbf{x}' \leftarrow \mathbf{x}' \oplus \mathbf{x}$. It can be seen that the error on the system S has propagated to the system S' , and $|\theta\rangle_{SS'}$ is a product state that can be rewritten as

$$|\theta\rangle_{SS'} = X^{e_X} Q_N(|\mathbf{u}\rangle_Z \otimes Z^{\mathbf{w}'} |\phi\rangle_I \otimes |\overline{\mathbf{v} \oplus \mathbf{v}'}\rangle_{X'}) \otimes X^{e_X \oplus e'_X} Q_N(|\mathbf{u}' \oplus \mathbf{u}\rangle_{Z'} \otimes |\overline{\mathbf{w}'}\rangle_{I'} \otimes |\overline{\mathbf{v}'}\rangle_{X'}). \quad (32)$$

Hence, the partial state of the system S is the same as in (25). Further, measuring the qubits of the ancilla system in the Pauli Z basis, we get $\mathbf{m} = P_N(\mathbf{u} \oplus \mathbf{u}', \mathbf{a}', \mathbf{x}') \oplus e_X \oplus e'_X \in \{0, 1\}^N$, for some random vectors $\mathbf{a}' \in \{0, 1\}^{|Z|}$ and $\mathbf{x}' \in \{0, 1\}^{|X|}$. \square

Two observations are in place here.

First, from (25), it follows that the frozen vector corresponding to $\mathcal{X} \subset S$ (original system) has changed to $\mathbf{v} \oplus \mathbf{v}'$, after the Steane's procedure. Further, the logical Z operator corresponding to $Z^{\mathbf{w}'}$ gets applied on S . However, since we know \mathbf{w}' , we can reverse this logical operation using (19). Hence, the logical information encoded in S has not been altered, due to the syndrome extraction.

The second observation concerns the SC decoding, which takes as input the measurement outcome $\mathbf{m} = P_N(\mathbf{u} \oplus \mathbf{u}', \mathbf{a}', \mathbf{x}') \oplus e_X \oplus e'_X$, and the frozen vector $\mathbf{u} \oplus \mathbf{u}'$. It produces an estimate of the information vector⁷ $(\mathbf{a}', \mathbf{x}')$, from which we can produce an estimate of the total error $e_X \oplus e'_X$. The vector \mathbf{a}' may be correctly estimated, owing to the fact that it corresponds to good virtual channels. Some of the \mathbf{x}' positions may be incorrectly estimated (see Section 2.2.2), but this does not matter, as the induced logical error corresponds to an X -type stabilizer operator, acting trivially on the code space.

Hence, assuming the vector \mathbf{a}' is decoded correctly, we also get the correct value of the total error $e_X \oplus e'_X$ (up to an X -type stabilizer operator). We then correct the S system by applying $X^{e_X \oplus e'_X}$, which will leave the error $X^{e'_X}$ (original error on S') on S after correction.

⁷Corresponding to the unfrozen virtual channels, see Fig. 3a. Note that the SC decoding estimates the inputs of the classical polar transform P_N , given a noisy version of the corresponding codeword.

This leftover error, may hopefully be corrected in the next round of correction, where we may similarly add another error from the ancilla system. However, note that the advantage of error correction is that it does not allow errors to accumulate and the only left error on the encoded state is due to the last round of error correction (which may be corrected, when the encoded logical state is eventually measured). Hence, we may stabilize logical qubits against noise, by doing error correction repeatedly⁸.

Z-Error Correction. The decoding of Z errors can be done similarly to the case of X errors as follows. To extract the syndrome for Z errors (see Fig. 4b), one needs an ancilla system S' prepared in a logical Z basis state,

$$|\widetilde{w'}\rangle_{S'} = Q_N(|u'\rangle_{Z'} \otimes |w'\rangle_{I'} \otimes |\bar{v'}\rangle_{X'}), \quad (33)$$

After preparing the state $|\widetilde{w'}\rangle_{S'}$ on ancilla system S' , the qubitwise $\text{CNOT}_{S' \rightarrow S}$ gate is applied on corresponding qubits of systems S and S' . Then, each qubit in the ancilla system S' is measured in the Pauli X basis. The measurement output m is a noisy codeword of the classical polar code $\mathcal{P}(N, \pi(\mathcal{X}), \pi(v))$, induced in X basis (Fig. 3b).

Lemma 4. Let e_Z and e'_Z be preparation errors that has happened on systems S and S' , respectively. Then, after the Steane's Z -error syndrome extraction, the state of the system S is given by

$$Z^{e_Z} |\widetilde{X^{w'}\phi}\rangle_S = Z^{e_Z} Q_N(|u \oplus u'\rangle_Z \otimes X^{w'} |\phi\rangle_I \otimes |\bar{v}\rangle_X). \quad (34)$$

Further, the measurement outcome is a noisy codeword of the classical polar code $\mathcal{P}(N, \pi(\mathcal{X}), \pi(v))$, with frozen set \mathcal{X} and frozen vector $\pi(v \oplus v')$, as follows,

$$m = P_N^\top(z', a', v \oplus v') \oplus e_Z \oplus e'_Z, \quad (35)$$

where $a' \in \{0, 1\}^{|\mathcal{Z}|}$ and $x' \in \{0, 1\}^{|\mathcal{X}|}$ are random vectors.

The proof of Lemma 4 is similar to that of Lemma 3, by expanding quantum states of systems S and S' in the Pauli X basis. Finally, based on the frozen vector $v \oplus v'$ and the noisy codeword m in (35), the SC decoder generates an estimate of a' , and in turn we can obtain an estimate of the error $e_Z \oplus e'_Z$ (up to a Z -type stabilizer operator).

⁸It is worth noticing that for topological or quantum LDPC codes, fault tolerant error correction needs the decoding operation to be applied on a time window, composed of several consecutive syndrome extractions, e.g., [11]. For Steane's fault tolerant error correction, decoding is simply applied on each extracted "syndrome" (recall the "syndrome" in this case is actually a noisy codeword).

3 \mathcal{Q}_1 codes: Quantum Polar Codes Encoding One Qubit

3.1 Definition of \mathcal{Q}_1 Codes

A \mathcal{Q}_1 code is defined as follows. We select an index $i \in \mathcal{S} := \{1, \dots, N\}$ to place the information qubit, that is, $\mathcal{I} = \{i\}$. All the indices before i belong to the frozen set \mathcal{Z} , that is, $\mathcal{Z} = \{1, \dots, i-1\}$, and all the indices after it belong to the frozen set \mathcal{X} , that is, $\mathcal{X} := \{i+1, \dots, N\}$. Further, we have frozen vectors $\mathbf{u} \in \{0, 1\}^{i-1}$ and $\mathbf{v} \in \{0, 1\}^{N-i}$. The CSS quantum polar code $Q(N, \mathcal{Z}, \mathcal{X}, |\mathbf{u}\rangle_{\mathcal{Z}}, |\mathbf{v}\rangle_{\mathcal{X}})$ is referred to as a \mathcal{Q}_1 code.

First, we note that the choice of the frozen sets \mathcal{Z} and \mathcal{X} (given the information qubit position i) is simply explained by the sequential nature of the decoding process, and the fact that only errors on position i need be corrected. To correct X errors, virtual channels are decoded in order, from 1 to N . Freezing a virtual channel $j > i$ in Z basis would be of no help in decoding the virtual channel i , while freezing it in X basis amounts to ignoring X errors that happen on it. A similar observation holds for Z errors, by noticing that in this case virtual channels are decoding in reversed (decreasing) order, from N to 1 (Fig. 3b).

Further, we observe that the family of \mathcal{Q}_1 codes, for which the information position is a power of two, that is, $i = 2^k, 0 \leq k \leq n$, is equivalent to the well-known Shor quantum error correcting codes [37, 38] (see also [40]). This follows from Lemma 5 below. Therefore, we refer to these codes as *Shor- \mathcal{Q}_1 codes*, or simply Shor codes, when no confusion is possible.

To observe this, we will use the decomposition $Q_N = (I_{2^k} \otimes Q_{2^{n-k}})(Q_{2^k} \otimes I_{2^{n-k}})$, for $0 \leq k \leq n$. This decomposition is illustrated in Fig. 5, where we have 2^{n-k} parallel Q_{2^k} blocks, followed by 2^k parallel $Q_{2^{n-k}}$ blocks. If one considers the quantum system \mathcal{S} as a vector of N qubits, the decomposition illustrated in Fig. 5 is equivalent to reshaping \mathcal{S} as a $2^k \times 2^{n-k}$ matrix of qubits, with columns filled in by consecutive qubits from the original vector, then applying Q_{2^k} on each column, and $Q_{2^{n-k}}$ on each row.

In Lemma 5 below, for the sake of simplicity, we consider \mathcal{Q}_1 codes, such that all the elements in \mathcal{Z} are frozen in the basis state $|0\rangle$, and all the elements in \mathcal{X} are frozen in the basis state $|+\rangle$. We denote these \mathcal{Q}_1 codes by $\mathcal{Q}_1(N, i)$.

Lemma 5. *For a given $i = 2^k, 0 \leq k \leq n$, the logical states $|\tilde{0}\rangle_{\mathcal{S}}$ and $|\tilde{1}\rangle_{\mathcal{S}}$ of the $\mathcal{Q}_1(N, i)$ code are as follows (up to a normalization factor),*

$$|\tilde{0}\rangle_{\mathcal{S}} = \bigotimes_{r=1}^{2^k} \left(\bigotimes_{c=1}^{2^{n-k}} |+\rangle_{r,c} + \bigotimes_{c=1}^{2^{n-k}} |-\rangle_{r,c} \right), \quad (36)$$

$$|\tilde{1}\rangle_{\mathcal{S}} = \bigotimes_{r=1}^{2^k} \left(\bigotimes_{c=1}^{2^{n-k}} |+\rangle_{r,c} - \bigotimes_{c=1}^{2^{n-k}} |-\rangle_{r,c} \right), \quad (37)$$

where r and c are row and column indexes, with \mathcal{S} being reshaped as a $2^k \times 2^{n-k}$ matrix of qubits.

Proof. For the logical state $|\tilde{0}\rangle_{\mathcal{S}}$, the first $i = 2^k$ inputs of the quantum polar transform Q_N are equal to $|0\rangle$, while the remaining $2^n - 2^k$ inputs are equal to $|+\rangle$ (see Fig. 5). Hence, each of the 2^{n-k} parallel Q_{2^k} unitaries in Fig. 5 acts trivially on its input state. Therefore, the input of the r -th $Q_{2^{n-k}}$ unitary, where $1 \leq r \leq 2^k$, is the quantum state $|0\rangle_{r,1} \bigotimes_{c=2}^{2^{n-k}} |+\rangle_{r,c}$. It follows that

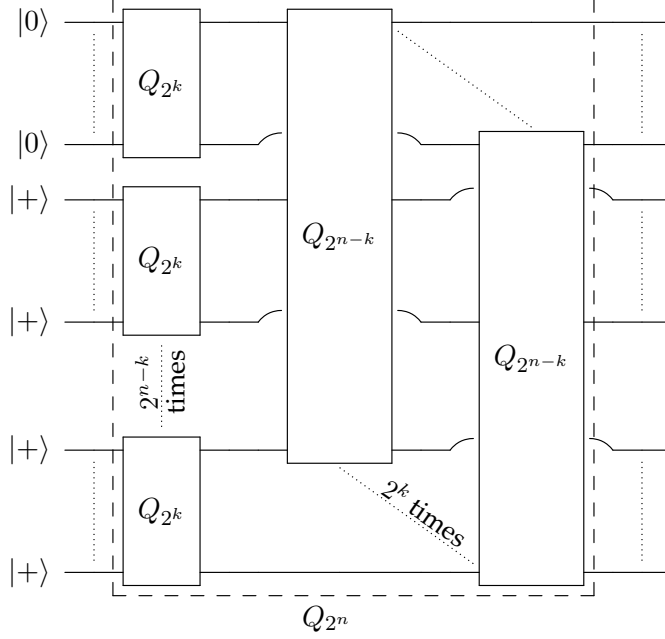


Fig. 5: Quantum polar transform decomposition, using $Q_{2^n} = (I_{2^k} \otimes Q_{2^{n-k}})(Q_{2^k} \otimes I_{2^{n-k}})$. Bent wires go under the blocks they cross. In case input qubits are prepared as shown on the left, the encoded state is the logical $|0\rangle$ state of a Shor code.

(omitting normalization factors),

$$|\tilde{0}\rangle_S = \otimes_{r=1}^{2^k} Q_{2^{n-k}} \left(|0\rangle_{r,1} \otimes_{c=2}^{2^{n-k}} |+\rangle_{r,c} \right) = \otimes_{r=1}^{2^k} Q_{2^{n-k}} \left((|+\rangle_{r,1} + |-\rangle_{r,1}) \otimes_{c=2}^{2^{n-k}} |+\rangle_{r,c} \right) \quad (38)$$

$$= \otimes_{r=1}^{2^k} \left(Q_{2^{n-k}} \left(\otimes_{c=1}^{2^{n-k}} |+\rangle_{r,c} \right) + Q_{2^{n-k}} \left(|-\rangle_{r,1} \otimes_{c=2}^{2^{n-k}} |+\rangle_{r,c} \right) \right) \quad (39)$$

$$= \otimes_{r=1}^{2^k} \left(\otimes_{c=1}^{2^{n-k}} |+\rangle_{r,c} + \otimes_{c=1}^{2^{n-k}} |-\rangle_{r,c} \right) \quad (40)$$

For the logical state $|\tilde{1}\rangle_S$, the inputs of Q_N are the same, except for input in position $i = 2^k$, which is equal to $|1\rangle$. Hence, for the first (top) Q_{2^n} unitary in Fig. 5, we get the state $Q_{2^n}(|0 \dots 01\rangle) = |1 \dots 11\rangle$. Therefore, the input of the r -th $Q_{2^{n-k}}$ unitary, where $1 \leq r \leq 2^k$, is the quantum state $|1\rangle_{r,1} \otimes_{c=2}^{2^{n-k}} |+\rangle_{r,c}$, and (37) follows as above, using $|1\rangle_{r,1} = |+\rangle_{r,1} - |-\rangle_{r,1}$ (omitting normalization factors). \square

3.2 Construction of \mathcal{Q}_1 Codes

The *construction* of a \mathcal{Q}_1 code refers to the choice of the information position i , which determines how well the code protects the encoded quantum information. Hence, the position i should be chosen in a way to optimize the code's decoding performance, depending on the specific noise model (*i.e.*, quantum channel). For \mathcal{Q}_1 codes, any information position $i \in \mathcal{S}$ may be chosen. For the subfamily of Shor- \mathcal{Q}_1 codes, the choice is restricted to positions $i = 2^k$, $0 \leq k \leq n$.

To determine the information position, recall from the previous section that only errors on position i need be decoded. Let W_Z and W_X be the classical channels induced in Z and X bases, respectively (Section 2.2.2). Let $P_e(W_Z^{(i)})$ and $P_e(W_X^{(\pi(i))})$ denote the error probability of the respective virtual channels⁹, corresponding to the information position i . Hence, the

⁹The error probability of a classical channel, is the probability of the maximum a posteriori estimate of the

logical error rate of the \mathcal{Q}_1 code, with respect to the information position i , is given by

$$P_e^L(i) = 1 - \left(1 - P_e\left(W_Z^{(i)}\right)\right) \left(1 - P_e\left(W_X^{(\pi(i))}\right)\right). \quad (41)$$

The information position i should be chosen so as to minimize the corresponding logical error rate in (41). Precisely, we have

$$i = \arg \min_{j=1, \dots, N} P_e^L(j), \quad \text{for } \mathcal{Q}_1 \text{ codes} \quad (42)$$

$$i = \arg \min_{j=2^0, \dots, 2^n} P_e^L(j), \quad \text{for Shor-}\mathcal{Q}_1 \text{ codes} \quad (43)$$

Numerical Results. Here, we provide numerical results for the construction of \mathcal{Q}_1 and Shor- \mathcal{Q}_1 codes, for the quantum depolarizing and quantum erasure channels.

The quantum depolarizing channel with physical error probability p , is a Pauli channel as in (20), with $P_I = 1 - p$, and $p_X = p_Y = p_Z = p/3$. We use density evolution [39] to estimate the error probability of virtual channels, *i.e.*, $P_e\left(W_Z^{(j)}\right)$ and $P_e\left(W_X^{(\pi(j))}\right)$, $j = 1, \dots, N$. The information positions for the \mathcal{Q}_1 and Shor- \mathcal{Q}_1 codes are then determined according to (42) and (43). Moreover, we consider the two constructions (or decoding strategies) from Section 2.2.2, that is, either using or ignoring the correlations between X and Z errors¹⁰.

The quantum erasure channel erases the input qubit, with some probability ε , or transmits it perfectly, with probability $1 - \varepsilon$. When a qubit is erased, it is replaced by a totally mixed state. Further, the channel also outputs a classical flag, which indicates whether the qubit has been erased ($|1\rangle_E$) or not ($|0\rangle_E$). Hence, it can be represented as a quantum operation as follows,

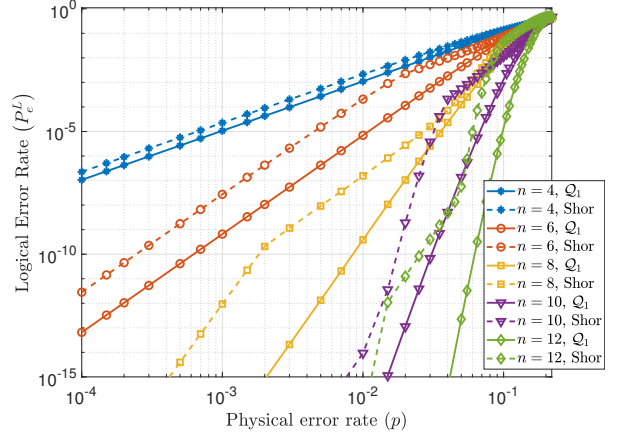
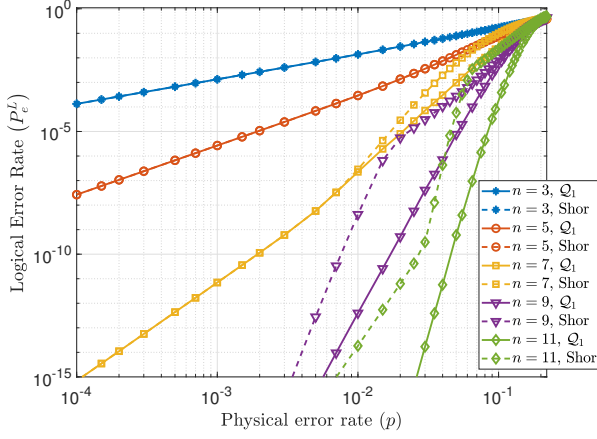
$$\mathcal{W}_E(\rho) = (1 - \varepsilon)|0\rangle\langle 0|_E \otimes \rho + \varepsilon|1\rangle\langle 1|_E \otimes \frac{\mathbb{1}}{2}. \quad (44)$$

It is easily seen that \mathcal{W}_E acts as a classical erasure channel with erasure probability ε in both Pauli Z and Pauli X basis. Hence, the induced channels W_X and W_Z are classical erasure channels, with erasure probability ε . The erasure probability of virtual channels ($P_e\left(W_Z^{(j)}\right)$ and $P_e\left(W_X^{(\pi(j))}\right)$, $j = 1, \dots, N$) can be computed analytically [31]. The information positions for the \mathcal{Q}_1 and Shor- \mathcal{Q}_1 codes are then determined according to (42) and (43). For this channel, the two construction strategies (using or ignoring correlations) are easily seen to be equivalent.

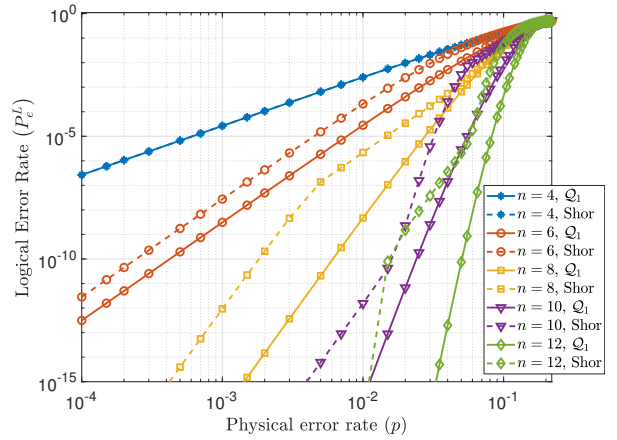
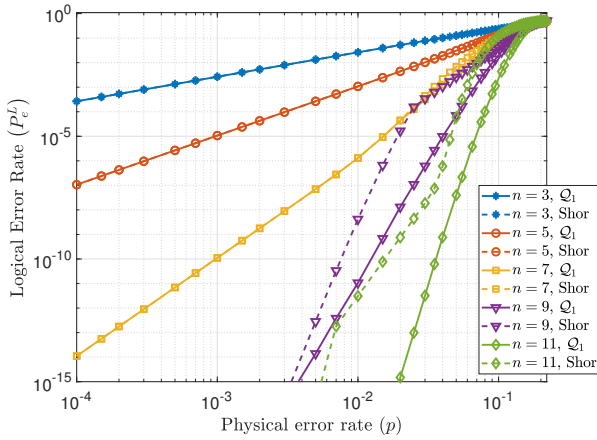
Considering the quantum depolarizing channel, Fig. 6 shows the logical error rate $P_e^L(i)$ vs. the physical error probability p , for the \mathcal{Q}_1 and Shor- \mathcal{Q}_1 codes, with information position determined according to (42) and (43). Note that for fixed codelength $N = 2^n$, the information position may vary depending on the physical error probability value. We consider the two decoding strategies mentioned above, namely, either using or ignoring the correlations between X and Z errors. It can be observed that using correlations yield (slightly) better decoding performance. Moreover, in both cases, we observe that the logical error rate of the \mathcal{Q}_1 code is in general lower than that of the Shor code, and the gap is increasing with increasing codelength (*i.e.*, number of polarization steps n). We emphasize that the gap in the decoding

channel input, conditional on the observed channel output, not being equal to the actual input.

¹⁰Here, ignoring correlations between X and Z errors may seem unfounded. We will provide the rationale for this in Section 5.2, paragraph “Prepared Codes”.



(a) Using correlations between X and Z errors. Left: n odd (for $n = 3, 5, 7$, \mathcal{Q}_1 and Shor curves virtually coincide). Right: n even.



(b) Ignoring correlations between X and Z errors. Left: n odd (for $n = 3, 5, 7$, \mathcal{Q}_1 and Shor curves virtually coincide). Right: n even (for $n = 4$, \mathcal{Q}_1 and Shor curves virtually coincide).

Fig. 6: Logical error rate of \mathcal{Q}_1 and Shor codes, for the depolarizing channel.

performance is due to the channel polarization phenomenon and not to the minimum distance (\mathcal{Q}_1 and Shor- \mathcal{Q}_1 codes have actually the same minimum distance, see below).

As just mentioned, the information position i may vary, depending on the physical error probability p . However, numerical results suggests that as p goes to zero, the information position i reaches a stable (constant) value. These values are reported in Table 1, for both decoding strategies (either using or ignoring correlations), and different values of n . We also report in Table 1 similar results for the quantum erasure channel (we omit the logical error rate curves for the quantum erasure channel, since they are of the same nature as the logical error rate curves in Fig. 6). It can be observed that for \mathcal{Q}_1 codes, the information position values reported in Table 1 depend on the noise model (depolarizing or erasure channel), as well as the decoding strategy (using or ignoring correlations).

Finally, we note that for a given n value, all \mathcal{Q}_1 and Shor codes with information positions given in Table 1 have the same minimum distance, which is reported on the last column of the table. The reported minimum distance is the minimum weight of logical X and Z operators, and can be computed by using (18) and (19).

Table 1: Best information positions for low error probabilities^(*)

Levels of Recursion (n)	Depolarizing Channel using correlations		Depolarizing Channel ignoring correlations		Erasure Channel		Min dist.
	Information position i for best \mathcal{Q}_1 and Shor- \mathcal{Q}_1 codes						
	\mathcal{Q}_1	Shor	\mathcal{Q}_1	Shor	\mathcal{Q}_1	Shor	
3	4 (6.8×10^{-2})	4 (2.0×10^{-1})	4 (1.0×10^{-3})	4 (1.0×10^{-3})	2 (5.0×10^{-1})	2 (5.0×10^{-1})	2
4	13 (2.0×10^{-1})	4 (2.0×10^{-1})	7 (9.0×10^{-4})	4 (2.0×10^{-1})	7 (5.0×10^{-1})	4 (5.0×10^{-1})	4
5	8 (2.0×10^{-1})	8 (2.0×10^{-1})	8 (2.0×10^{-1})	8 (2.0×10^{-1})	4 (2.0×10^{-1})	4 (5.0×10^{-1})	4
6	50 (1.6×10^{-1})	8 (1.8×10^{-2})	23 (1.4×10^{-1})	8 (8.8×10^{-2})	23 (5.0×10^{-1})	8 (4.0×10^{-2})	8
7	16 (8.0×10^{-3})	16 (2.0×10^{-1})	16 (1.8×10^{-2})	16 (2.0×10^{-1})	8 (2.6×10^{-2})	8 (1.9×10^{-1})	8
8	199 (1.4×10^{-2})	16 (2.0×10^{-3})	91 (6.2×10^{-2})	16 (4.0×10^{-3})	87 (2.6×10^{-1})	16 (6.0×10^{-3})	16
9	32 (1.0×10^{-3})	32 (1.6×10^{-2})	32 (2.0×10^{-3})	32 (2.4×10^{-2})	16 (5.0×10^{-3})	16 (4.4×10^{-2})	16
10	806 (6.0×10^{-5})	32 (3.0×10^{-4})	363 (6.2×10^{-2})	32 (6.0×10^{-4})	343 (9.0×10^{-2})	32 (1.0×10^{-3})	32
11	96 (3.0×10^{-4})	64 (4.0×10^{-3})	96 (6.4×10^{-4})	64 (6.3×10^{-3})	32 (1.0×10^{-3})	32 (1.4×10^{-2})	32
12	3222 (6.0×10^{-5})	64 (6.0×10^{-5})	1451 (6.6×10^{-2})	64 (1.0×10^{-4})	1367 (4.4×10^{-2})	64 (2.4×10^{-4})	64

(*) For the depolarizing channel, we consider physical error rates $p \in [10^{-5}, 2 \times 10^{-1}]$ (note that the coherent information of the channel vanishes for $p \approx 0.1893$). Reported information position values are constant for physical error rates $p \in [10^{-5}, p_0]$. The value of p_0 is reported between round brackets, under the value of i (tiny font size). Similarly, for the quantum erasure channel, we consider channel erasure probability values $\varepsilon \in [10^{-5}, 5 \times 10^{-1}]$. Reported information position values are constant for channel erasure probabilities $\varepsilon \in [10^{-5}, \varepsilon_0]$, where the value of ε_0 is reported between round brackets, under the value of i .

4 Measurement-Based Preparation of Logical \mathcal{Q}_1 Code States

As \mathcal{Q}_1 codes have excellent error-correction capabilities, under fast SC decoding, they might represent an interesting option for FTQC. Fault-tolerant logical state preparation is required to initialize the computation, but also to perform fault-tolerant error correction, using the Steane procedure presented in Section 2.2.3.

For preparing a logical code state, we may assume that all the qubits are frozen in either Z or X basis. Indeed, for the logical state $|\tilde{0}\rangle_{\mathcal{S}}$, the information position i is frozen in $|0\rangle$. Therefore, we may consider that the virtual channels with indexes in the set $\mathcal{Z} = \{1, \dots, i\}$ are frozen in a Pauli Z basis state, and those with indexes in the set $\mathcal{X} = \{i+1, \dots, N\}$ are frozen in a Pauli X basis state. Similarly, for the logical state $|\tilde{+}\rangle_{\mathcal{S}}$, the information position i is frozen in $|+\rangle$. Thus, we may consider $\mathcal{Z} = \{1, \dots, i-1\}$ and $\mathcal{X} = \{i, \dots, N\}$.

Consequently, we consider here the preparation of general \mathcal{Q}_1 code states, with frozen sets $\mathcal{Z} = \{1, \dots, i\}$ and $\mathcal{X} = \{i+1, \dots, N\}$, for some arbitrary $1 \leq i \leq N$, where $N = 2^n$, $n > 0$. Further, since our preparation procedure is recursive, we will need to clearly indicate in the notation the length of the prepared \mathcal{Q}_1 code state. To do so, we will use the notation $i(n) := i$, $\mathcal{Z}(n) := \mathcal{Z}$, and $\mathcal{X}(n) := \mathcal{X}$. Therefore, we want to prepare the following N -qubit \mathcal{Q}_1 code state

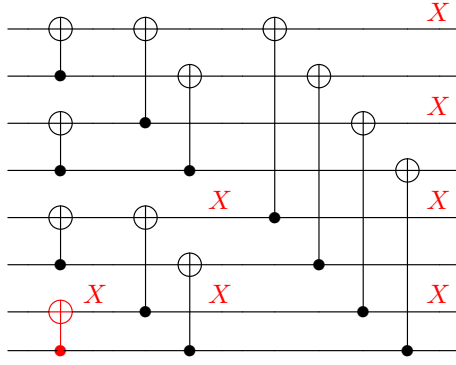


Fig. 7: Propagation of X errors through the quantum polar transform.

on the system $\mathcal{S} = \{1, \dots, N\}$,

$$|q_N\rangle_{\mathcal{S}} := Q_N(|\mathbf{u}, \bar{\mathbf{v}}\rangle_{\mathcal{S}}) = Q_N(|\mathbf{u}\rangle_{\mathcal{Z}(n)} \otimes |\bar{\mathbf{v}}\rangle_{\mathcal{X}(n)}), \quad (45)$$

where $\mathbf{u} \in \{0, 1\}^{|\mathcal{Z}(n)|}$ and $\mathbf{v} \in \{0, 1\}^{|\mathcal{X}(n)|}$ ($\mathcal{Z}(n) = \{1, \dots, i(n)\}$, $\mathcal{X}(n) = \{i(n) + 1, \dots, N\}$).

A straightforward way to prepare the \mathcal{Q}_1 code state in (45) is to implement the circuit of the quantum polar transform directly. However, this is not a fault-tolerant preparation, when the noise is present, as an error on a qubit (caused by the failure of a CNOT gate for example) may propagate to many qubits through the CNOT gates, that are applied afterwards. This is illustrated in Fig. 7. Hence, we need to find other methods for preparing \mathcal{Q}_1 code states.

Here, we propose a new method of preparation of \mathcal{Q}_1 code states, based on quantum measurements, where two-qubit Pauli measurements are applied recursively, on *equivalent code states* (see below). We describe our method in two steps. First, we describe our measurement based procedure, assuming no errors occur during the procedure, and show that it does indeed prepare a \mathcal{Q}_1 code state as in (45), where frozen sets $\mathcal{Z}(n)$ and $\mathcal{X}(n)$ are given before the procedure, but frozen states $|\mathbf{u}\rangle_{\mathcal{Z}(n)}$ and $|\bar{\mathbf{v}}\rangle_{\mathcal{X}(n)}$ are only known when the procedure completes. Then, we investigate the fault tolerance of the proposed procedure, under the effect of errors (*i.e.*, noisy gates and measurements). We show that our procedure can be made fault-tolerant by incorporating an error detection mechanism, exploiting the redundancy in the measurement outcomes, at each level of recursion.

Before describing the proposed method, we first observe from (10)-(11) that the Z and X type stabilizer groups of $|q_N\rangle_{\mathcal{S}}$ in (45) are given by,

$$S_Z = \{(-1)^{\mathbf{z} \cdot \mathbf{u}} Z^{P_N^{\top}(\mathbf{z}, 0)} \mid \mathbf{z} \in \{0, 1\}^{i(n)}\} \quad (46)$$

$$S_X = \{(-1)^{\mathbf{x} \cdot \mathbf{v}} X^{P_N(0, \mathbf{x})} \mid \mathbf{x} \in \{0, 1\}^{N-i(n)}\} \quad (47)$$

Further, consider two \mathcal{Q}_1 code states, $|q_N^1\rangle$ and $|q_N^2\rangle$, with the same $i(n)$ value. We refer to $|q_N^1\rangle$ and $|q_N^2\rangle$, as *equivalent \mathcal{Q}_1 code states*. Hence, frozen sets $\mathcal{Z}(n)$ and $\mathcal{X}(n)$ are the same, however, the corresponding frozen states ($|\mathbf{u}_1\rangle_{\mathcal{Z}(n)}, |\bar{\mathbf{v}}_1\rangle_{\mathcal{X}(n)}$) and ($|\mathbf{u}_2\rangle_{\mathcal{Z}(n)}, |\bar{\mathbf{v}}_2\rangle_{\mathcal{X}(n)}$) may be different. Using (46) and (47), it follows that $|q_N^1\rangle$ and $|q_N^2\rangle$ have the same stabilizer groups S_Z and S_X , modulo the sign factors, and one can get one state from another by applying Pauli unitaries only.

4.1 Measurement-Based Preparation Without Noise

Our preparation procedure is based on the recursive application of two-qubit Pauli measurements, where at each level of recursion, either Pauli $Z \otimes Z$ or Pauli $X \otimes X$ measurements are performed on equivalent code states.

We first give the measurement based procedure to prepare a \mathcal{Q}_1 code state of length $N = 2^n$, with information position $i(n) \in \{1, \dots, N\}$, assuming that we are given two equivalent \mathcal{Q}_1 code states of length $N/2 = 2^{n-1}$, with information position $i(n-1) \in \{1, \dots, N/2\}$. Applied recursively, our procedure can be used to prepare a \mathcal{Q}_1 code state of given length N and $i(n)$ value, as detailed in Section 4.1.3.

To prepare a \mathcal{Q}_1 code state of length N , *i.e.*, a state $|q_N\rangle_{\mathcal{S}}$ as in (45), we suppose that we have been given two equivalent \mathcal{Q}_1 code states of length $N/2$,

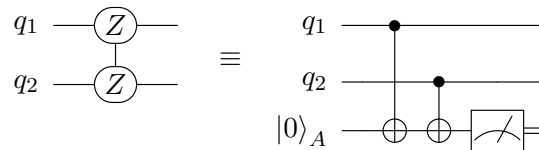
$$|q_{\frac{N}{2}}^1\rangle_{\mathcal{S}_1} := Q_{\frac{N}{2}} |u_1, \bar{v}_1\rangle_{\mathcal{S}_1}, \quad (48)$$

$$|q_{\frac{N}{2}}^2\rangle_{\mathcal{S}_2} := Q_{\frac{N}{2}} |u_2, \bar{v}_2\rangle_{\mathcal{S}_2}, \quad (49)$$

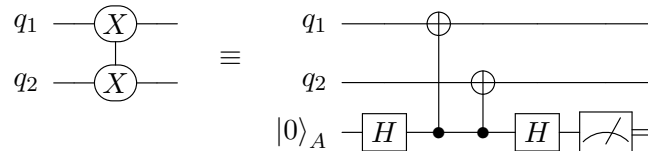
where $u_1, u_2 \in \{0, 1\}^{i(n-1)}$ and $v_1, v_2 \in \{0, 1\}^{\frac{N}{2}-i(n-1)}$, with $1 \leq i(n-1) \leq N/2$. Here, \mathcal{S}_1 and \mathcal{S}_2 are two $N/2$ -qubit systems, and we further identify \mathcal{S} to the joint system $\mathcal{S}_1\mathcal{S}_2$. We distinguish between the following two cases (detailed in the following two sections):

- (1) Preparation using Pauli $Z \otimes Z$ measurements. In this case, the prepared $|q_N\rangle_{\mathcal{S}}$ state has information position $i(n) = i(n-1) + N/2$.
- (2) Preparation using Pauli $X \otimes X$ measurements. In this case, the prepared $|q_N\rangle_{\mathcal{S}}$ state has information position $i(n) = i(n-1)$.

Fig. 8 shows the shorthand notation that will be used in the rest of the paper for Pauli $Z \otimes Z$ and Pauli $X \otimes X$ measurements, as well as the quantum circuits implementing these measurements.



(a) Pauli $Z \otimes Z$ measurement: shorthand notation (left) and quantum circuit implementing the Pauli $Z \otimes Z$ measurement (right).



(b) Pauli $X \otimes X$ measurement: shorthand notation (left) and quantum circuit implementing the Pauli $X \otimes X$ measurement (right).

Fig. 8: Two-qubit Pauli measurements: shorthand notation and quantum circuits implementing the measurements.

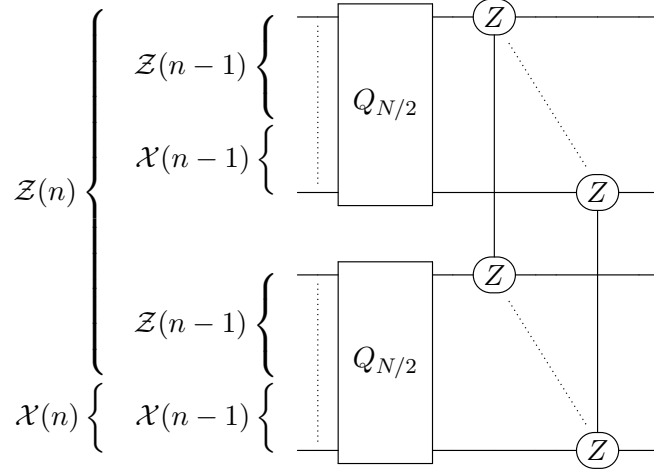


Fig. 9: Preparation using Pauli $Z \otimes Z$ measurements ($i(n) = i(n-1) + \frac{N}{2} \in \{\frac{N}{2} + 1, \dots, N\}$).

4.1.1 Preparation Using Pauli $Z \otimes Z$ Measurements

In this case, our procedure consists in performing qubitwise Pauli $Z \otimes Z$ measurements on corresponding qubits of systems \mathcal{S}_1 and \mathcal{S}_2 in (48) and (49), as illustrated in Fig. 9.

Taking $i(n) = i(n-1) + N/2$, we may consider $\mathcal{Z}(n)$ as the disjoint union of \mathcal{S}_1 and the $\mathcal{Z}(n-1)$ part of \mathcal{S}_2 , and $\mathcal{X}(n)$ as being equal to the $\mathcal{X}(n-1)$ part of \mathcal{S}_2 (see Fig. 9).

In Lemma 6 below, we show that after performing the qubitwise Pauli $Z \otimes Z$ measurements, we prepare the desired \mathcal{Q}_1 code state from (45), on system $\mathcal{S} = \mathcal{S}_1\mathcal{S}_2$.

Lemma 6. *The measurement outcome of qubitwise Pauli $Z \otimes Z$ measurements on systems \mathcal{S}_1 and \mathcal{S}_2 in (48) and (49), respectively, is equal to*

$$\mathbf{m} = P_{\frac{N}{2}}(\mathbf{u}', \mathbf{x}) \in \{0, 1\}^{\frac{N}{2}}, \quad (50)$$

where $\mathbf{u}' = \mathbf{u}_1 \oplus \mathbf{u}_2 \in \{0, 1\}^{i(n-1)}$ and $\mathbf{x} \in \{0, 1\}^{\frac{N}{2}-i(n-1)}$ is a random vector. Further, after the measurement, we are left with the \mathcal{Q}_1 code state on the joint system $\mathcal{S}_1\mathcal{S}_2$, depending on \mathbf{x} , as follows

$$|q_N\rangle_{\mathcal{S}_1\mathcal{S}_2} = Q_N(|\mathbf{u}, \bar{\mathbf{v}}\rangle_{\mathcal{S}_1\mathcal{S}_2}), \quad (51)$$

where $\mathbf{u} = (\mathbf{u}', \mathbf{x}, \mathbf{u}_2) \in \{0, 1\}^{i(n)}$ and $\mathbf{v} = \mathbf{v}_1 \oplus \mathbf{v}_2 \in \{0, 1\}^{N-i(n)}$, and where \mathbf{x} can be determined from the measurement outcome \mathbf{m} in (50) as,

$$\mathbf{x} = P_{\frac{N}{2}}(\mathbf{m})|_{\mathcal{X}(n-1)}. \quad (52)$$

Proof. Expanding the quantum state $|\bar{\mathbf{v}}_1\rangle_{\mathcal{X}(n-1)}$ in (48) in the Pauli Z basis, and using (7), we get, up to a normalization factor,

$$|q_{\frac{N}{2}}^1\rangle_{\mathcal{S}_1} = \sum_{\mathbf{x}_1 \in \{0, 1\}^{\frac{N}{2}-i(n-1)}} (-1)^{\mathbf{v}_1 \cdot \mathbf{x}_1} |P_{\frac{N}{2}}(\mathbf{u}_1, \mathbf{x}_1)\rangle_{\mathcal{S}_1}. \quad (53)$$

Similarly, we may also expand the quantum state $|q_{N/2}^2\rangle_{\mathcal{S}_2}$ in the Pauli Z basis. Further, we consider the circuit in Fig. 8a to perform qubitwise Pauli $Z \otimes Z$ measurements, which are done in the following two steps.

- (1) We first take an $(N/2)$ -qubit ancilla state $|0\rangle_{\mathcal{S}_3}$, and then apply qubitwise CNOT gates, $\text{CNOT}_{\mathcal{S}_1 \rightarrow \mathcal{S}_3}$ and $\text{CNOT}_{\mathcal{S}_2 \rightarrow \mathcal{S}_3}$. This gives the following joint quantum state on $\mathcal{S}_1 \mathcal{S}_2 \mathcal{S}_3$.

$$|\eta\rangle_{\mathcal{S}_1 \mathcal{S}_2 \mathcal{S}_3} = \sum_{\mathbf{x}_1, \mathbf{x}_2 \in \{0,1\}^{\frac{N}{2}-i(n-1)}} (-1)^{\mathbf{v}_1 \cdot \mathbf{x}_1 + \mathbf{v}_2 \cdot \mathbf{x}_2} |P_{\frac{N}{2}}(\mathbf{u}_1, \mathbf{x}_1)\rangle_{\mathcal{S}_1} |P_{\frac{N}{2}}(\mathbf{u}_2, \mathbf{x}_2)\rangle_{\mathcal{S}_2} |P_{\frac{N}{2}}(\mathbf{u}_1 \oplus \mathbf{u}_2, \mathbf{x}_1 \oplus \mathbf{x}_2)\rangle_{\mathcal{S}_3}. \quad (54)$$

- (2) Then, we measure each qubit in the ancilla system \mathcal{S}_3 in the Pauli Z basis. From (54), the measurement outcome gives a binary vector of length $N/2$ as follows,

$$\mathbf{m} = P_{\frac{N}{2}}(\mathbf{u}', \mathbf{x}) \in \{0,1\}^{\frac{N}{2}}, \quad (55)$$

where $\mathbf{u}' = \mathbf{u}_1 \oplus \mathbf{u}_2$ and \mathbf{x} is a random vector $\{0,1\}^{\frac{N}{2}-i(n)}$. Further, from (54) and (55), the state of the joint system $\mathcal{S}_1 \mathcal{S}_2$ after the measurements is as follows

$$|\eta'\rangle_{\mathcal{S}_1 \mathcal{S}_2} = \sum_{\substack{\mathbf{x}_1, \mathbf{x}_2 \in \{0,1\}^{\frac{N}{2}-i(n-1)} \\ \mathbf{x}_1 \oplus \mathbf{x}_2 = \mathbf{x}}} (-1)^{\mathbf{v}_1 \cdot \mathbf{x}_1 + \mathbf{v}_2 \cdot \mathbf{x}_2} |P_{\frac{N}{2}}(\mathbf{u}_1, \mathbf{x}_1)\rangle_{\mathcal{S}_1} |P_{\frac{N}{2}}(\mathbf{u}_2, \mathbf{x}_2)\rangle_{\mathcal{S}_2} \quad (56)$$

It can be seen as follows that the quantum state $|\eta'\rangle_{\mathcal{S}_1 \mathcal{S}_2}$ is the \mathcal{Q}_1 code state $|q_N\rangle_{\mathcal{S}_1 \mathcal{S}_2}$ in (51),

$$\begin{aligned} |\eta'\rangle_{\mathcal{S}_1 \mathcal{S}_2} &= \sum_{\substack{\mathbf{x}_1, \mathbf{x}_2 \in \{0,1\}^{\frac{N}{2}-i(n-1)} \\ \mathbf{x}_1 \oplus \mathbf{x}_2 = \mathbf{x}}} (-1)^{\mathbf{v}_1 \cdot \mathbf{x}_1 + \mathbf{v}_2 \cdot \mathbf{x}_2} |P_{\frac{N}{2}}(\mathbf{u}_1, \mathbf{x}_1)\rangle_{\mathcal{S}_1} |P_{\frac{N}{2}}(\mathbf{u}_2, \mathbf{x}_2)\rangle_{\mathcal{S}_2} \\ &= \sum_{\mathbf{x}_2} (-1)^{\mathbf{v}_1 \cdot (\mathbf{x} \oplus \mathbf{x}_2) + \mathbf{v}_2 \cdot \mathbf{x}_2} |P_{\frac{N}{2}}(\mathbf{u}' \oplus \mathbf{u}_2, \mathbf{x} \oplus \mathbf{x}_2)\rangle_{\mathcal{S}_1} |P_{\frac{N}{2}}(\mathbf{u}_2, \mathbf{x}_2)\rangle_{\mathcal{S}_2} \\ &= (-1)^{\mathbf{v}_1 \cdot \mathbf{x}} \sum_{\mathbf{x}_2} (-1)^{(\mathbf{v}_1 + \mathbf{v}_2) \cdot \mathbf{x}_2} |P_N(\mathbf{u}', \mathbf{x}, \mathbf{u}_2, \mathbf{x}_2)\rangle_{\mathcal{S}_1 \mathcal{S}_2} \\ &= Q_N(|\mathbf{u}', \mathbf{x}, \mathbf{u}_2, \overline{\mathbf{v}_1 \oplus \mathbf{v}_2}\rangle_{\mathcal{S}_1 \mathcal{S}_2}) \end{aligned} \quad (57)$$

where in the second equality, we have used $\mathbf{u}_1 = \mathbf{u}' \oplus \mathbf{u}_2$ and $\mathbf{x}_1 = \mathbf{x} \oplus \mathbf{x}_2$, and in the third equality, we have used $P_N(\mathbf{a}, \mathbf{b}) = (P_{\frac{N}{2}}(\mathbf{a} \oplus \mathbf{b}), P_{\frac{N}{2}}(\mathbf{b}))$, $\mathbf{a}, \mathbf{b} \in \{0,1\}^{\frac{N}{2}}$, using the recursion of the classical polar transform given in Fig. 1a.

Finally, from (55), we have that $P_{\frac{N}{2}}(\mathbf{m}) = (\mathbf{u}', \mathbf{x}) \in \{0,1\}^{\frac{N}{2}}$ (using $P_N^2 = I$). Hence, it follows that $\mathbf{x} = P_{\frac{N}{2}}(\mathbf{m})|_{\mathcal{X}(n-1)}$, as desired. \square

4.1.2 Preparation Using Pauli $X \otimes X$ Measurements

In this case, our procedure consists in performing qubitwise Pauli $X \otimes X$ measurements on corresponding qubits of systems \mathcal{S}_1 and \mathcal{S}_2 in (48) and (49), as illustrated in Fig. 10.

Taking $i(n) = i(n-1)$, we may consider $\mathcal{Z}(n)$ as equal to the $\mathcal{Z}(n-1)$ part of \mathcal{S}_1 , and $\mathcal{X}(n)$ as the disjoint union of the $\mathcal{X}(n-1)$ part of \mathcal{S}_1 and \mathcal{S}_2 (see Fig. 10).

Lemma 7 below states that after performing the qubitwise Pauli $X \otimes X$ measurements, we get the desired \mathcal{Q}_1 code state from (45), on system $\mathcal{S} = \mathcal{S}_1 \mathcal{S}_2$.

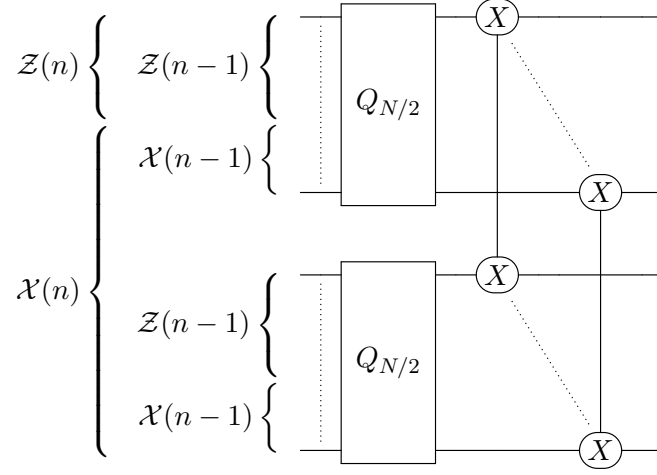


Fig. 10: Preparation using Pauli $X \otimes X$ measurements ($i(n) = i(n-1) \in \{1, \dots, \frac{N}{2}\}$)

Lemma 7. *The measurement outcome of qubitwise Pauli $X \otimes X$ measurements on systems \mathcal{S}_1 and \mathcal{S}_2 in (48) and (49), respectively, is equal to*

$$\mathbf{m} = P_{\frac{N}{2}}^\top(\mathbf{z}, \mathbf{v}') \in \{0, 1\}^{\frac{N}{2}}, \quad (58)$$

where $\mathbf{z} \in \{0, 1\}^{i(n)}$ is a random vector, and $\mathbf{v}' = \mathbf{v}_1 \oplus \mathbf{v}_2 \in \{0, 1\}^{\frac{N}{2}-i(n)}$. Further, after the measurement, we are left with the \mathcal{Q}_1 code state on the joint system $\mathcal{S}_1\mathcal{S}_2$, as follows

$$|q_N\rangle_{\mathcal{S}_1\mathcal{S}_2} := Q_N|\mathbf{u}, \bar{\mathbf{v}}\rangle_{\mathcal{S}_1\mathcal{S}_2}, \quad (59)$$

where $\mathbf{u} = \mathbf{u}_1 \oplus \mathbf{u}_2 \in \{0, 1\}^{i(n)}$ and $\mathbf{v} = (\mathbf{v}_1, \mathbf{z}, \mathbf{v}') \in \{0, 1\}^{N-i(n)}$, and where \mathbf{z} can be determined from the measurement outcome \mathbf{m} in (58), as follows

$$\mathbf{z} = P_{\frac{N}{2}}^\top(\mathbf{m})|_{\mathcal{Z}(n-1)}. \quad (60)$$

We skip the proof of Lemma 7 as it can be done similar to Lemma 6, by expanding $|q_{\frac{N}{2}}^1\rangle_{\mathcal{S}_1}$ and $|q_{\frac{N}{2}}^2\rangle_{\mathcal{S}_2}$, respectively in (48) and (49), in the Pauli X basis instead of Pauli Z basis.

4.1.3 Recursion

Here, we describe the preparation of a \mathcal{Q}_1 code state of length $N = 2^n$ and given information position $i(n)$, by recursively applying qubitwise Pauli measurements as in Fig. 9 and Fig. 10 (see also Fig. 11 below).

Basically, for any given N , one can prepare the corresponding \mathcal{Q}_1 code state, using our procedure on two equivalent \mathcal{Q}_1 code states of length $\frac{N}{2}$, wherein \mathcal{Q}_1 code states of length $\frac{N}{2}$ are prepared, using our procedure on two equivalent \mathcal{Q}_1 code states of length $\frac{N}{4}$ and so on. Finally, for $N = 1$, we may initialize our procedure by preparing all the qubits in the Pauli Z basis. We may assume that the initialization is done by performing single qubit Pauli- Z measurements on each qubit of the N qubit quantum system $\mathcal{S} = \{1, \dots, N\}$, therefore, making the entire procedure measurement based.

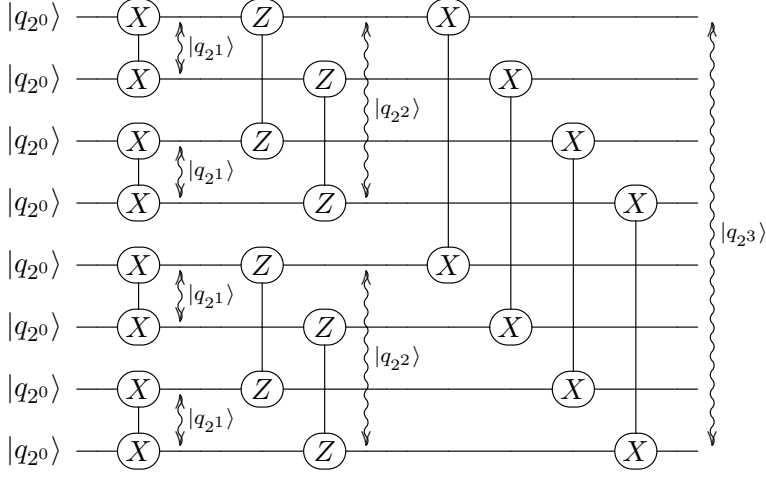


Fig. 11: Example of measurement based preparation for $N = 8$ ($n = 3$) and $i(n) = 3$. Here $i(2) = 3$ and $i(1) = 1$. Quantum states $|q_{2^k}\rangle$ appearing in several places are not the same state, but they are equivalent \mathcal{Q}_1 code states of length 2^k . For $k = 0$, $|q_{2^0}\rangle$ simply denotes a Pauli Z basis state (which needs not be the same for all qubits).

In more details, the above recursive procedure is implemented as follows. Given $N = 2^n$ and information position $i(n) \in \{1, \dots, N\}$, we start by determining the information positions $i(k) \in \{1, \dots, 2^k\}$, for $k = n - 1, \dots, 1$, by using the following descendant recursion.

$$i(k) = \begin{cases} i(k+1) - 2^k, & \text{if } i(k+1) > 2^k \\ i(k+1), & \text{otherwise} \end{cases} \quad (61)$$

We then initialize an N qubit system $\mathcal{S} = \{1, \dots, N\}$ in a Pauli Z basis state, corresponding to some $\mathbf{u} \in \{0, 1\}^n$. As mentioned before, this can be done by performing single qubit Pauli Z measurements on each qubit of \mathcal{S} . We shall consider the initial state as N instances of \mathcal{Q}_1 code states $|q_{2^0}\rangle_{\mathcal{S}^0(j)}$, where $j = 1, \dots, N$, and where $\mathcal{S}^0(j) := \{j\}$ is a quantum system containing only one qubit.

Next, we perform n levels of recursion, indexed by $k = 1, \dots, n$, and indicated by wavy arrows in Fig. 11. At the k -th level of recursion, we proceed as follows.

- We group the 2^{n-k+1} instances of \mathcal{Q}_1 code states $|q_{2^{k-1}}\rangle_{\mathcal{S}^{k-1}(j)}$ (from the previous level) into 2^{n-k} pairs. We then apply the same two-qubit Pauli measurement on each pair.
- Precisely, according to Lemmas 6 and 7, if $i(k) > 2^{k-1}$, we perform qubitwise Pauli $Z \otimes Z$ measurements, otherwise we perform qubitwise Pauli $X \otimes X$ measurements.
- This gives us 2^{n-k} instances of \mathcal{Q}_1 code states $|q_{2^k}\rangle_{\mathcal{S}^k(j)}$, where $\mathcal{S}^k(j)$ refers to the quantum system $\{\mathcal{S}^{k-1}(2j-1), \mathcal{S}^{k-1}(2j)\}$, for $j = 1, \dots, 2^{n-k}$.

At the final level of recursion $k = n$, we have only one \mathcal{Q}_1 code state $|q_{2^n}\rangle_{\mathcal{S}^n(1)}$, where $\mathcal{S}^n(1) = \mathcal{S} = \{1, \dots, N\}$.

Remark. Let $b_1 \cdots b_n$ be the binary representation of the integer $i(n) - 1$, with b_1 being the least significant bit, that is, $i(n) - 1 = \sum_{k=1}^n b_k 2^{k-1}$. It can be easily seen that $i(k) > 2^{k-1}$ if and only if $b_k = 1$. Hence, at the k -th level of recursion, we perform qubitwise Pauli $Z \otimes Z$ measurements if $b_k = 1$, and qubitwise Pauli $X \otimes X$ measurements if $b_k = 0$. For the example in Fig. 11, $n = 3$ and $i(n) = 3$, hence $b_1 b_2 b_3 = 010$, giving Pauli $X \otimes X$ measurements for the first and the third level of recursion, and Pauli $Z \otimes Z$ measurements for the second one.

4.2 Fault-tolerant measurement based preparation under the effect of noise

In this section, we consider our measurement based procedure under the effect of noise, and we provide generalizations of Lemmas 6 and 7. Precisely, we assume that we are given noisy versions of \mathcal{Q}_1 code states in (48) and (49)

$$|q_{\frac{N}{2}}^1\rangle_{\mathcal{S}_1} = X^{e_X^1} Z^{e_Z^1} Q_{\frac{N}{2}} |\mathbf{u}_1, \bar{\mathbf{v}}_1\rangle_{\mathcal{S}_1}, \quad (62)$$

$$|q_{\frac{N}{2}}^2\rangle_{\mathcal{S}_2} = X^{e_X^2} Z^{e_Z^2} Q_{\frac{N}{2}} |\mathbf{u}_2, \bar{\mathbf{v}}_2\rangle_{\mathcal{S}_2}, \quad (63)$$

where $\mathbf{u}_1, \mathbf{u}_2 \in \{0, 1\}^{i(n-1)}$, $\mathbf{v}_1, \mathbf{v}_2 \in \{0, 1\}^{\frac{N}{2}-i(n-1)}$, and the errors $e_X^1, e_Z^1, e_X^2, e_Z^2 \in \{0, 1\}^{\frac{N}{2}}$ are unknown.

For the sake of clarity, we first assume that we apply perfect qubitwise Pauli measurements, without errors, on corresponding qubits of systems \mathcal{S}_1 and \mathcal{S}_2 , in (62) and (63). In Lemmas 8 and 9 below, we provide the final errors on the prepared \mathcal{Q}_1 code states after the Pauli $Z \otimes Z$ and the Pauli $X \otimes X$ measurements, respectively. We later observe that Lemmas 8 and 9 can be easily extended for noisy Pauli measurements, considering a Pauli error model.

Further, we observe from Lemmas 8 and 9 that random vectors \mathbf{x} and \mathbf{z} (generated within the measurement operations) can no longer be determined from the measurement outcome \mathbf{m} using (52) and (60), as in the error free case above. Determining these vectors is important, in order to know the frozen states of the prepared \mathcal{Q}_1 code states, after the respective qubitwise Pauli measurements. To solve this problem, we incorporate an error detection method with our procedure, where if an error is detected, we discard the \mathcal{Q}_1 code state, and if it is not detected, we determine \mathbf{x} and \mathbf{z} according to (52) and (60), respectively.

4.2.1 Preparation Using Noisy Pauli $Z \otimes Z$ Measurements

We now state and prove the generalization of Lemma 6 to the noisy case.

Lemma 8 (Noisy version of Lemma 6). *The measurement outcome of qubitwise Pauli $Z \otimes Z$ measurements on systems \mathcal{S}_1 and \mathcal{S}_2 , respectively in (62) and (63), is equal to*

$$\mathbf{m} = P_{\frac{N}{2}}(\mathbf{u}', \mathbf{x}) \oplus \mathbf{e}_X \in \{0, 1\}^{\frac{N}{2}}, \quad (64)$$

where $\mathbf{u}' = \mathbf{u}_1 \oplus \mathbf{u}_2 \in \{0, 1\}^{i(n-1)}$, $\mathbf{x} \in \{0, 1\}^{\frac{N}{2}-i(n-1)}$ is a random vector, and $\mathbf{e}_X = \mathbf{e}_X^1 \oplus \mathbf{e}_X^2 \in \{0, 1\}^{\frac{N}{2}}$. Further, after the measurement, we get a noisy version of the \mathcal{Q}_1 code state in (51) as follows,

$$|q_N\rangle_{\mathcal{S}_1 \mathcal{S}_2} = X^{\tilde{\mathbf{e}}_X} Z^{\tilde{\mathbf{e}}_Z} Q_N |\mathbf{u}, \bar{\mathbf{v}}\rangle_{\mathcal{S}_1 \mathcal{S}_2}, \quad (65)$$

where $\mathbf{u} = (\mathbf{u}', \mathbf{x}, \mathbf{u}_2) \in \{0, 1\}^{i(n)}$ and $\mathbf{v} = \mathbf{v}_1 \oplus \mathbf{v}_2 \in \{0, 1\}^{N-i(n)}$, as in Lemma 6, and where the final errors are as follows¹¹,

$$\tilde{\mathbf{e}}_X = (\mathbf{e}_X^1, \mathbf{e}_X^2) \in \{0, 1\}^N \quad (66)$$

$$\tilde{\mathbf{e}}_Z = (\mathbf{e}_Z^1, \mathbf{e}_Z^2) \in \{0, 1\}^N. \quad (67)$$

Proof. We proceed as in the proof of Lemma 6, by expanding $|q_{\frac{N}{2}}^1\rangle_{S_1}$ in (62) in the Z basis. We may write, up to a normalization factor,

$$|q_{\frac{N}{2}}^1\rangle_{S_1} = \sum_{\mathbf{x}_1 \in \{0,1\}^{\frac{N}{2}-i(n-1)}} (-1)^{\mathbf{v}_1 \cdot \mathbf{x}_1 + \mathbf{e}_Z^1 \cdot P_{\frac{N}{2}}(\mathbf{u}_1, \mathbf{x}_1)} |P_{\frac{N}{2}}(\mathbf{u}_1, \mathbf{x}_1) \oplus \mathbf{e}_X^1\rangle_{S_1}. \quad (68)$$

Similarly, we may also expand $|q_{\frac{N}{2}}^2\rangle_{S_2}$ in (63) in Z basis. Further, similar to the proof of Lemma 6, we perform qubitwise Pauli measurements in the following two steps.

- (1) We first take an $(N/2)$ -qubit ancilla state $|0\rangle_{S_3}$, and then apply qubitwise CNOT gates $\text{CNOT}_{S_1 \rightarrow S_3}$ and $\text{CNOT}_{S_2 \rightarrow S_3}$. This gives the following joint quantum state on $S_1 S_2 S_3$ (where summation indices $\mathbf{x}_1, \mathbf{x}_2 \in \{0, 1\}^{\frac{N}{2}-i(n-1)}$).

$$|\eta\rangle_{S_1 S_2 S_3} = \sum_{\mathbf{x}_1, \mathbf{x}_2} (-1)^{\mathbf{v}_1 \cdot \mathbf{x}_1 + \mathbf{e}_Z^1 \cdot P_{\frac{N}{2}}(\mathbf{u}_1, \mathbf{x}_1)} (-1)^{\mathbf{v}_2 \cdot \mathbf{x}_2 + \mathbf{e}_Z^2 \cdot P_{\frac{N}{2}}(\mathbf{u}_2, \mathbf{x}_2)} |P_{\frac{N}{2}}(\mathbf{u}_1, \mathbf{x}_1) \oplus \mathbf{e}_X^1\rangle_{S_1} |P_{\frac{N}{2}}(\mathbf{u}_2, \mathbf{x}_2) \oplus \mathbf{e}_X^2\rangle_{S_2} |P_{\frac{N}{2}}(\mathbf{u}_1 \oplus \mathbf{u}_2, \mathbf{x}_1 \oplus \mathbf{x}_2) \oplus \mathbf{e}_X^1 \oplus \mathbf{e}_X^2\rangle_{S_3}. \quad (69)$$

- (2) Then, we measure each qubit in the ancilla system S_3 in the Pauli Z basis. From (69), the measurement outcome gives a binary vector of length $\frac{N}{2}$ as follows,

$$\mathbf{m} = P_{\frac{N}{2}}(\mathbf{u}', \mathbf{x}) \oplus \mathbf{e}_X \in \{0, 1\}^{\frac{N}{2}}, \quad (70)$$

where $\mathbf{u}' = \mathbf{u}_1 \oplus \mathbf{u}_2$, $\mathbf{x} \in \{0, 1\}^{\frac{N}{2}-i(n)}$ is a random vector, and $\mathbf{e}_X = \mathbf{e}_X^1 \oplus \mathbf{e}_X^2$. Further, from (69) and (70), the state of the joint system $S_1 S_2$ after the measurements is as follows,

$$|\eta'\rangle_{S_1 S_2} = \sum_{\substack{\mathbf{x}_1, \mathbf{x}_2 \\ \mathbf{x}_1 \oplus \mathbf{x}_2 = \mathbf{x}}} (-1)^{\mathbf{v}_1 \cdot \mathbf{x}_1 + \mathbf{e}_Z^1 \cdot P_{\frac{N}{2}}(\mathbf{u}_1, \mathbf{x}_1)} (-1)^{\mathbf{v}_2 \cdot \mathbf{x}_2 + \mathbf{e}_Z^2 \cdot P_{\frac{N}{2}}(\mathbf{u}_2, \mathbf{x}_2)} |P_{\frac{N}{2}}(\mathbf{u}_1, \mathbf{x}_1) \oplus \mathbf{e}_X^1\rangle_{S_1} |P_{\frac{N}{2}}(\mathbf{u}_2, \mathbf{x}_2) \oplus \mathbf{e}_X^2\rangle_{S_2}. \quad (71)$$

It can be seen as follows that the quantum state $|\eta'\rangle_{S_1 S_2}$ in (71) is the \mathcal{Q}_1 code state $|q_N\rangle_{S_1 S_2}$ in (65),

$$\begin{aligned} |\eta'\rangle_{S_1 S_2} &= \sum_{\mathbf{x}_2} (-1)^{\mathbf{v}_1 \cdot \mathbf{x} + (\mathbf{v}_1 + \mathbf{v}_2) \cdot \mathbf{x}_2 + \mathbf{e}_Z^1 \cdot P_{\frac{N}{2}}(\mathbf{u}' \oplus \mathbf{u}_2, \mathbf{x} \oplus \mathbf{x}_2) + \mathbf{e}_Z^2 \cdot P_{\frac{N}{2}}(\mathbf{u}_2, \mathbf{x}_2)} \\ &\quad |P_{\frac{N}{2}}(\mathbf{u}' \oplus \mathbf{u}_2, \mathbf{x} \oplus \mathbf{x}_2) \oplus \mathbf{e}_X^1\rangle_{S_1} |P_{\frac{N}{2}}(\mathbf{u}_2, \mathbf{x}_2) \oplus \mathbf{e}_X^2\rangle_{S_2} \\ &= (-1)^{\mathbf{v}_1 \cdot \mathbf{x}} \sum_{\mathbf{x}_2} (-1)^{(\mathbf{v}_1 + \mathbf{v}_2) \cdot \mathbf{x}_2 + (\mathbf{e}_Z^1, \mathbf{e}_Z^2) \cdot P_N(\mathbf{u}', \mathbf{x}, \mathbf{u}_2, \mathbf{x}_2)} |P_N(\mathbf{u}', \mathbf{x}, \mathbf{u}_2, \mathbf{x}_2) \oplus (\mathbf{e}_X^1, \mathbf{e}_X^2)\rangle_{S_1 S_2} \\ &= X^{\tilde{\mathbf{e}}_X} Z^{\tilde{\mathbf{e}}_Z} Q_N |(\mathbf{u}', \mathbf{x}, \mathbf{u}_2, \overline{\mathbf{v}_1 \oplus \mathbf{v}_2})\rangle_{S_1 S_2}, \end{aligned} \quad (72)$$

where in the first equality, we have used $\mathbf{u}_1 = \mathbf{u}' \oplus \mathbf{u}_2$ and $\mathbf{x}_1 = \mathbf{x} \oplus \mathbf{x}_2$, and the second equality follows from the recursion of polar transform given in Fig. 1a, and final errors are given as $\tilde{\mathbf{e}}_X = (\mathbf{e}_X^1, \mathbf{e}_X^2)$ and $\tilde{\mathbf{e}}_Z = (\mathbf{e}_Z^1, \mathbf{e}_Z^2)$. \square

¹¹We have previously used the tilde notation for logical code states. Here $\tilde{\mathbf{e}}_X = (\mathbf{e}_X^1, \mathbf{e}_X^2)$ simply means that $\tilde{\mathbf{e}}_X$ is the concatenation of \mathbf{e}_X^1 and \mathbf{e}_X^2 errors, and similarly for $\tilde{\mathbf{e}}_Z$.

Fault Tolerance. According to (66) and (67), the final X and Z errors in the prepared N qubit state $|q_N\rangle_{\mathcal{S}_1\mathcal{S}_2}$ are simply given by the X and Z errors that have happened in the given $\frac{N}{2}$ qubit states $|q_{N/2}^1\rangle_{\mathcal{S}_1}$ and $|q_{N/2}^2\rangle_{\mathcal{S}_2}$, in (62) and (63), respectively. Therefore, the measurement based preparation does not propagate errors to an increasing number of qubits on $|q_N\rangle_{\mathcal{S}_1\mathcal{S}_2}$, hence, it is fault-tolerant.

Extension to Noisy Measurements. Further, Lemma 8 can be extended for noisy Pauli $Z \otimes Z$ measurements, considering a Pauli error model as follows (see also Section 5). For the CNOT gates in step (1) of Pauli $Z \otimes Z$ measurements in the proof of Lemma 8, we assume that Pauli errors may happen on the qubits acted on by each CNOT gate¹² (after the gate is applied). For the single qubit Pauli Z measurements used in step (2), we assume that the measurement outcome may be flipped, or equivalently, a Pauli X error may happen on the measured qubit, before the measurement. For the above error model, we simply add an extra X error in the measurement outcome \mathbf{m} in (64), representing the errors caused on the system \mathcal{S}_3 by noisy $\text{CNOT}_{\mathcal{S}_1 \rightarrow \mathcal{S}_3}$, $\text{CNOT}_{\mathcal{S}_2 \rightarrow \mathcal{S}_3}$ gates and single qubit Pauli Z measurements. Further, we may also add extra X and Z errors in the prepared state on $\mathcal{S}_1\mathcal{S}_2$ in (65), caused by noisy $\text{CNOT}_{\mathcal{S}_1 \rightarrow \mathcal{S}_3}$ and $\text{CNOT}_{\mathcal{S}_2 \rightarrow \mathcal{S}_3}$ gates, on systems \mathcal{S}_1 and \mathcal{S}_2 , respectively. It is easily seen that these errors do not propagate to other qubits, thus the fault tolerance of our procedure remains unaffected by considering noisy Pauli $Z \otimes Z$ measurements.

Estimation of the Z -Basis Frozen State. Note that the prepared code state in (65) has Z -basis frozen state $|\mathbf{u}\rangle_{\mathcal{Z}(n)} = |\mathbf{u}', \mathbf{x}, \mathbf{u}_2\rangle_{\mathcal{Z}(n)}$, where $\mathbf{x} \in \{0, 1\}^{\frac{N}{2} - i(n-1)}$ is an unknown random vector. Hence, to know the prepared \mathcal{Q}_1 code state in (65), we need to determine the random vector \mathbf{x} . Note that (52) used to determine \mathbf{x} in the error free case, is no longer valid for the measurement outcome \mathbf{m} in (64), due to the unknown error e_X . We propose below a method to determine \mathbf{x} , based on error detection, and taking advantage of the redundancy in the measurements.

After getting the measurement outcome \mathbf{m} in (64), we can determine the syndrome of the error term $e_X = e_X^1 \oplus e_X^2$. Precisely, we have

$$P_{\frac{N}{2}}(e_X)|_{\mathcal{Z}(n-1)} = P_{\frac{N}{2}}(\mathbf{m})|_{\mathcal{Z}(n-1)} \oplus \mathbf{u}'. \quad (73)$$

Note that \mathbf{m} and \mathbf{u}' vectors in the right-hand side term are known. Hence, we distinguish the following two cases.

[Zero Syndrome] If $P_{\frac{N}{2}}(e_X)|_{\mathcal{Z}(n-1)} = 0$, either no error occurred ($e_X = 0$), or it is not detected. Hence, we estimate the value of \mathbf{x} according to (52). Precisely, we determine

$$\hat{\mathbf{x}} = P_{\frac{N}{2}}(\mathbf{m})|_{\mathcal{X}(n-1)}, \quad (74)$$

where the hat notation indicates an estimate value, which may be different from the actual one (if $e_X \neq 0$, we may have $\hat{\mathbf{x}} \neq \mathbf{x}$).

Proposition 1 below gives the X error generated on the prepared state, in case an undetected non-trivial error ($e_X \neq 0$) leads to a wrong estimation of \mathbf{x} ($\hat{\mathbf{x}} \neq \mathbf{x}$).

¹²The specific error model, e.g., whether the errors on the two qubits acted on by the gate are correlated or not, the error probability, etc., does not matter here.

[Non-Zero Syndrome] If $P_{\frac{N}{2}}(e_X)|_{\mathcal{Z}(n-1)} \neq 0$, the prepared state is discarded and restarted by taking fresh \mathcal{Q}_1 code states of length $N/2$.

Proposition 1. Consider an error $e_X \in \{0, 1\}^{\frac{N}{2}}$ such that $P_{\frac{N}{2}}(e_X)|_{\mathcal{Z}(n-1)} = 0$, and let \hat{x} be defined as in (74). Then,

$$\hat{x} = x \oplus P_{\frac{N}{2}}(e_X)|_{\mathcal{X}(n-1)} \quad (75)$$

and with respect to \hat{x} , the joint system in (65) can be written as follows,

$$|q_N\rangle_{\mathcal{S}_1\mathcal{S}_2} = X^{\tilde{e}_X^2} Z^{\tilde{e}_Z} Q_N |(\mathbf{u}', \hat{x}, \mathbf{u}_2, \overline{\mathbf{v}_1 \oplus \mathbf{v}_2})\rangle_{\mathcal{S}_1\mathcal{S}_2}, \quad (76)$$

where the final X error is $\tilde{e}_X^2 = (e_X^2, e_X^2)$.

Proof. Equality (75) follows easily from (74) and (64). Further, we may write $|q_N\rangle_{\mathcal{S}_1\mathcal{S}_2}$ in (65), with respect to \hat{x} as follows,

$$\begin{aligned} |q_N\rangle_{\mathcal{S}_1\mathcal{S}_2} &= X^{\tilde{e}_X} Z^{\tilde{e}_Z} Q_N |(\mathbf{u}', x, \mathbf{u}_2, \overline{\mathbf{v}_1 \oplus \mathbf{v}_2})\rangle \\ &= X^{\tilde{e}_X} Z^{\tilde{e}_Z} \sum_{\mathbf{x}_2} (-1)^{(\mathbf{v}_1 \oplus \mathbf{v}_2) \cdot \mathbf{x}_2} |P_N(\mathbf{u}', \hat{x} \oplus P_{\frac{N}{2}}(e_X)|_{\mathcal{X}(n-1)}, \mathbf{u}_2, \overline{\mathbf{v}_1 \oplus \mathbf{v}_2})\rangle \\ &= X^{\tilde{e}_X} Z^{\tilde{e}_Z} \sum_{\mathbf{x}_2} (-1)^{(\mathbf{v}_1 \oplus \mathbf{v}_2) \cdot \mathbf{x}_2} X^{(e_X, 0)} |P_N(\mathbf{u}', \hat{x}, \mathbf{u}_2, \mathbf{x}_2)\rangle \\ &= X^{\tilde{e}_X^2} Z^{\tilde{e}_Z} Q_N |(\mathbf{u}', \hat{x}, \mathbf{u}_2, \overline{\mathbf{v}_1 \oplus \mathbf{v}_2})\rangle, \end{aligned} \quad (77)$$

where in the second equality, we have expanded the quantum state in the Pauli Z basis and used (75), in the third equality we have used $e_X = P_{\frac{N}{2}}(\mathbf{0}, P_{\frac{N}{2}}(e_X)|_{\mathcal{X}(n-1)})$, and finally, in the fourth equality, we have that $\tilde{e}_X^2 = \tilde{e}_X \oplus (e_X, \mathbf{0}) = (e_X^2, e_X^2)$. \square

We note that, under the hypothesis of Proposition 1, we have

$$\hat{x} = x \Leftrightarrow P_{\frac{N}{2}}(e_X)|_{\mathcal{Z}(n-1)} = P_{\frac{N}{2}}(e_X)|_{\mathcal{X}(n-1)} = 0 \Leftrightarrow e_X = 0 \Leftrightarrow e_X^1 = e_X^2. \quad (78)$$

The above proposition also implies that an undetected non-trivial error ($e_X \neq 0$) may cause a propagation of X errors from the \mathcal{S}_2 to the \mathcal{S}_1 system, since the final X error on the joint system $\mathcal{S}_1\mathcal{S}_2$ becomes $\tilde{e}_X^2 = (e_X^2, e_X^2)$. However, during the recursive preparation procedure, the X error on the prepared state can be detected in a subsequent level of recursion, when Pauli $Z \otimes Z$ measurements are performed again. Hence, the X error that is left on the final prepared state, at the end of recursion, is only due to the last recursion levels, which we expect can be corrected under SC decoding.

4.2.2 Preparation Using Noisy Pauli $X \otimes X$ Measurements

We state below the generalization of Lemma 7 to the noisy case.

Lemma 9 (Noisy version of Lemma 7). *The measurement outcome of qubitwise Pauli $X \otimes X$ measurements on systems \mathcal{S}_1 and \mathcal{S}_2 , respectively in (62) and (63), is equal to*

$$\mathbf{m} = P_{\frac{N}{2}}^\top(\mathbf{z}, \mathbf{v}') \oplus \mathbf{e}_Z \in \{0, 1\}^{\frac{N}{2}}, \quad (79)$$

where $\mathbf{z} \in \{0, 1\}^{i(n-1)}$ is a random vector, $\mathbf{v}' = \mathbf{v}_1 \oplus \mathbf{v}_2 \in \{0, 1\}^{\frac{N}{2}-i(n-1)}$, and $\mathbf{e}_Z = \mathbf{e}_Z^1 \oplus \mathbf{e}_Z^2 \in \{0, 1\}^{\frac{N}{2}}$. Further, after the measurement, we get a noisy version of the \mathcal{Q}_1 code state in (59) as follows,

$$|q_N\rangle_{S_1 S_2} = X^{\tilde{\mathbf{e}}_X} Z^{\tilde{\mathbf{e}}_Z} Q_N |\mathbf{u}, \bar{\mathbf{v}}\rangle_{S_1 S_2}, \quad (80)$$

where $\mathbf{u} = \mathbf{u}_1 \oplus \mathbf{u}_2 \in \{0, 1\}^{i(n)}$ and $\mathbf{v} = (\mathbf{v}_1, \mathbf{z}, \mathbf{v}') \in \{0, 1\}^{N-i(n)}$, as in Lemma 7, and the final errors are as follows,

$$\tilde{\mathbf{e}}_X = (\mathbf{e}_X^1, \mathbf{e}_X^2) \in \{0, 1\}^N, \quad (81)$$

$$\tilde{\mathbf{e}}_Z = (\mathbf{e}_Z^1, \mathbf{e}_Z^2) \in \{0, 1\}^N. \quad (82)$$

We omit the proof of Lemma 9 as it can be done similar to the proof of Lemma 8, by expanding $|q_{N/2}^1\rangle_{S_1}$ and $|q_{N/2}^2\rangle_{S_2}$, respectively in (62) and (63), in the Pauli X basis instead of the Pauli Z basis, and using the observation that the CNOT gate acts as the reversed XOR in the Pauli X basis. Similar to Section 4.2.1 above, Lemma 9 can be extended for noisy Pauli $X \otimes X$ measurements, considering a Pauli error model.

We need to determine the random vector $\mathbf{z} \in \{0, 1\}^{i(n-1)}$ to know the prepared \mathcal{Q}_1 code state in (80), which can not be done using (60) due to the unknown error \mathbf{e}_Z in the measurement outcome \mathbf{m} in (79). The vector \mathbf{z} is determined based on an error detection method as follows.

Estimation of the X -Basis Frozen State. The prepared code state in (80) has X -basis frozen state $|\bar{\mathbf{v}}\rangle_{\mathcal{X}(n)} = |\overline{\mathbf{v}_1, \mathbf{z}, \mathbf{v}'}\rangle_{\mathcal{X}(n)}$, where $\mathbf{z} \in \{0, 1\}^{i(n-1)}$ is an unknown random vector. Hence, we need to determine the random vector \mathbf{z} to know the prepared \mathcal{Q}_1 code state, which cannot be done using (60), due to the unknown error \mathbf{e}_Z in the measurement outcome \mathbf{m} in (79). The vector \mathbf{z} is determined based on an error detection method as follows.

After getting the measurement outcome \mathbf{m} in (79), we determine the syndrome of the error term $\mathbf{e}_Z = \mathbf{e}_Z^1 \oplus \mathbf{e}_Z^2$, by using

$$P_{\frac{N}{2}}^\top(\mathbf{e}_Z)|_{\mathcal{X}(n-1)} = P_{\frac{N}{2}}^\top(\mathbf{m})|_{\mathcal{X}(n-1)} \oplus \mathbf{v}'. \quad (83)$$

Then, we distinguish the following two cases.

[Zero Syndrome] If $P_{\frac{N}{2}}^\top(\mathbf{e}_Z)|_{\mathcal{X}(n-1)} = 0$, either no error occurred ($\mathbf{e}_Z = 0$), or it is not detected. Hence, we estimate the value of \mathbf{z} according to (60). Precisely, we determine

$$\hat{\mathbf{z}} = P_{\frac{N}{2}}^\top(\mathbf{m})|_{\mathcal{Z}(n-1)}, \quad (84)$$

where the hat notation indicates an estimate value.

Proposition 2 below gives the Z error generated on the prepared state, in case an undetected non-trivial error ($\mathbf{e}_Z \neq 0$) leads to a wrong estimation of \mathbf{z} ($\hat{\mathbf{z}} \neq \mathbf{z}$).

[Non-Zero Syndrome] If $P_{\frac{N}{2}}^\top(\mathbf{e}_Z)|_{\mathcal{X}(n-1)} \neq 0$, the prepared state is discarded and restarted by taking fresh \mathcal{Q}_1 code states of length $N/2$.

Proposition 2. Consider an error $e_Z \in \{0, 1\}^{\frac{N}{2}}$ such that $P_{\frac{N}{2}}^\top(e_Z)|_{\mathcal{X}(n-1)} = 0$, and let \hat{z} be defined as in (84). Then,

$$\hat{z} = z \oplus P_{\frac{N}{2}}^\top(e_Z)|_{\mathcal{Z}(n-1)} \quad (85)$$

and with respect to \hat{z} , the joint system in (80) can be written as follows,

$$|q_N\rangle_{\mathcal{S}_1\mathcal{S}_2} = X^{\tilde{e}_X} Z^{\tilde{e}_Z^1} Q_N |u_1 \oplus u_2, \overline{v_1, z, v'}\rangle_{\mathcal{S}_1\mathcal{S}_2}, \quad (86)$$

where the final Z error is $\tilde{e}_Z^1 = (e_Z^1, e_Z^1)$.

We skip the proof of Proposition 2, as it can be done similarly to that of Proposition 1, above.

5 Numerical Results

In this section, we present our numerical results regarding the preparation and the logical error rate performance of Q_1 code states, under the effect of noise. We start by presenting first the noise model used to generate errors during the simulation of the measurement-based preparation procedure and the Steane error-correction scheme. Note that we consider the implementation of Pauli $Z \otimes Z$ and Pauli $X \otimes X$ measurements according to circuits in Fig. 8a and Fig. 8b, respectively. However, for the Pauli $X \otimes X$ measurement in Fig. 8b, we consider the initialization in Pauli Z basis followed by the Hadamard gate as one operation, corresponding to the initialization in Pauli X basis, and similarly, we consider the last Hadamard gate followed by the Pauli X measurement as one operation, corresponding to a Pauli X measurement.

5.1 Noise model

According to the above assumptions, we only need noise models for initialization operations and single-qubit measurements, in either Z or X basis, and CNOT gates. We consider the following types of errors, corresponding to the circuit based depolarizing noise model from [11]. The probability parameter p below, is referred to as the *physical error rate*.

- (1) The noisy initialization in Pauli Z basis is equal to perfectly initializing a qubit in a Pauli Z basis state, then applying a Pauli X error on the qubit, with probability p . Similarly, the noisy initialization in Pauli X basis is equal to perfectly initializing a qubit in a Pauli X basis state, then applying a Pauli Z error on the qubit, with probability p .
- (2) The noisy Pauli Z measurement is equal to first applying a Pauli X error, with probability p , on the qubit we want to measure, and then applying the perfect Pauli Z measurement. Similarly, the noisy Pauli X measurement is equal to first applying a Pauli Z error, with probability p , and then applying the perfect Pauli X measurement.
- (3) The noisy CNOT gate is equal to the perfect CNOT followed by a two-qubit depolarizing channel, with error probability p . Precisely, after the perfect CNOT, any one of the 15 two qubit Pauli errors $I \otimes X, I \otimes Y, I \otimes Z, X \otimes I, X \otimes X, X \otimes Y, X \otimes Z, Y \otimes I, Y \otimes X, Y \otimes Y, Y \otimes Z, Z \otimes I, Z \otimes X, Z \otimes Y, Z \otimes Z$, may occur with probability $\frac{p}{15}$.

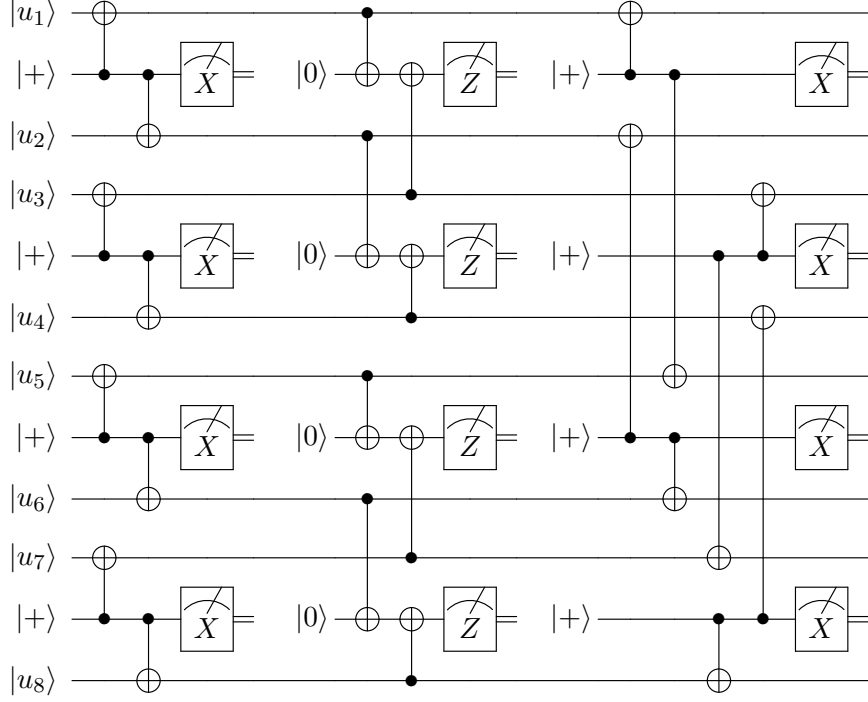


Fig. 12: Measurement based preparation for the \mathcal{Q}_1 code in Fig. 11 ($N = 8, i(n) = 3$), with Pauli $Z \otimes Z$ and Pauli $X \otimes X$ measurements implemented according to Fig. 8a and Fig. 8b. Initialization operations are shown as ket states. For single-qubit measurement operations, the Pauli basis is also indicated. Initialization operations, measurements, and CNOT gates are assumed to be noisy, according to the model from Section 5.1. Note that errors are generated only by the above noisy operations (we do not consider errors that might occur while the qubits are idle). Error detection is performed after each recursion level (one round of measurements of the four ancilla qubits), and the procedure is restarted from the beginning if an error is detected. Error detection after the first level of recursion is useless, hence it is not performed.

5.2 Simulation of the Preparation Procedure

Consider the \mathcal{Q}_1 code state $|q_N\rangle_{\mathcal{S}}$ on the $N = 2^n$ qubit system $\mathcal{S} = \{1, \dots, N\}$ in (45). To prepare $|q_N\rangle_{\mathcal{S}}$, we first initialize the N qubits in a Pauli Z basis state (using the noisy initialization defined above), and then follow the recursive procedure in Section 4.1.3. During the recursive procedure, initialization operations, CNOT gates, and single-qubit measurements are replaced by their noisy versions, and errors generated at some point by noisy operations are propagated throughout the rest of the procedure. If an error is detected at any recursion level (according to the error detection methods in Sections 4.2.1 and 4.2.2), then we discard the whole procedure and restart from the beginning, by initializing the N qubits in a Pauli Z basis state. See also the example in Fig. 12.

At the end of recursion, we have the knowledge of the $|u\rangle_{\mathcal{Z}(n)}$ and $|v\rangle_{\mathcal{X}(n)}$, hence the knowledge of prepared \mathcal{Q}_1 code state. Further, we also know the total X and Z type errors on the prepared state, which we will use for simulating Steane's syndrome extraction in Section 5.3.

Further, we determine the preparation rate of the measurement based procedure as follows. We run the preparation procedure $R > 0$ times, and denote by t be the number of times the

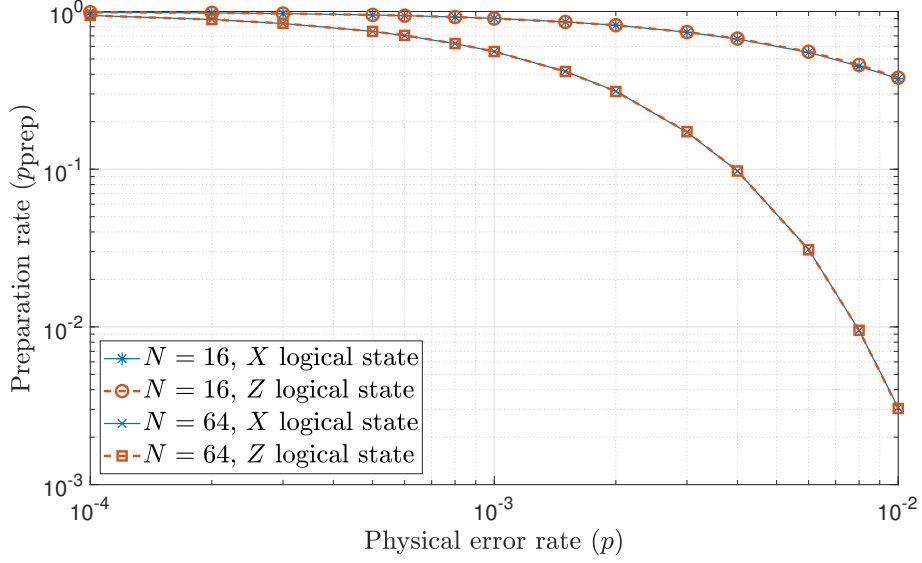


Fig. 13: Preparation rate for the logical X and logical Z code states of \mathcal{Q}_1 codes ($N = 16, i = 7$) and ($N = 64, i = 23$).

preparation completed (that is, no error has been detected during the preparation procedure). Then, the preparation rate, denoted by p_{prep} , is defined as follows,

$$p_{\text{prep}} = \frac{t}{R}. \quad (87)$$

Prepared Codes. We consider \mathcal{Q}_1 codes of length $N = 16$ and $N = 64$ qubits. We choose the information position i according to the results in Table 1 (best positions of the corresponding lengths, for sufficiently low error rate), assuming a depolarizing noise model and ignoring correlations between X and Z errors. Thus, for $N = 16$, we take the information position $i = 7$, and for $N = 64$, we take $i = 23$.

The fact that the \mathcal{Q}_1 code construction ignores correlations between X and Z errors is due to the Steane error correction. Indeed, X and Z errors are corrected independently, considering ancilla states prepared in either a logical X basis state $|\widetilde{w'}\rangle_{S'}$, or a logical Z basis state $|\widetilde{w'}\rangle_{S'}$, respectively (Section 2.2.3). During the X -error correction step (Fig. 4a), Z errors that happened on the ancilla system S' while preparing $|\widetilde{w'}\rangle_{S'}$, are copied to the original system S . Similarly, during the Z -error correction step (Fig. 4b), X errors that happened on the ancilla system S' while preparing $|\widetilde{w'}\rangle_{S'}$, are copied to S . Clearly, these X and Z errors are decorrelated, since they happened during the preparation of different logical states.

Fig. 13 shows the preparation rate p_{prep} , for the logical Z and logical X code states, with respect to the physical error rate p . Here, the total number of runs is $R = 10^5$.

We observe that p_{prep} is symmetric, in the sense that it is virtually the same for the X and Z logical states (the corresponding curves are superimposed), for both \mathcal{Q}_1 codes. Further, p_{prep} is non-zero for sufficiently low p and it approaches to 1 as p goes to zero, for both \mathcal{Q}_1 codes. However, p_{prep} is much lower for $N = 64, i = 23$, compared to $N = 16, i = 7$, especially at higher values of p . This is expected, as for $N = 64$ it is more likely that we detect an error, hence, discard the preparation, compared to $N = 16$.

5.3 Logical Error Rates

In this section, we determine logical X and Z error rates of \mathcal{Q}_1 codes, based on the Steane's error correction procedure. We consider a \mathcal{Q}_1 code of length N , with information position i , and make use of the notation from Section 3, namely, $\mathcal{I} = \{i\}$, $\mathcal{Z} = \{1, \dots, i-1\}$, $\mathcal{X} = \{i+1, \dots, N\}$, and $\mathcal{S} = \mathcal{Z} \cup \mathcal{I} \cup \mathcal{X}$.

Logical X Error Rate. To determine the logical X error rate, we prepare a logical Pauli Z basis code state $|\tilde{w}\rangle_{\mathcal{S}} = Q_N(|\mathbf{u}\rangle_{\mathcal{Z}} \otimes |w\rangle_{\mathcal{I}} \otimes |\bar{\mathbf{v}}\rangle_{\mathcal{X}})$, $w \in \{0, 1\}$, that we want to protect against X errors. Further, we prepare a logical Pauli X basis code state $|\tilde{w'}\rangle_{\mathcal{S'}} = Q_N(|\mathbf{u'}\rangle_{\mathcal{Z'}} \otimes |\bar{w'}\rangle_{\mathcal{I'}} \otimes |\bar{\mathbf{v'}}\rangle_{\mathcal{X'}})$, $w' \in \{0, 1\}$, to be used as the ancilla system for syndrome extraction (see Fig. 4a.)

The logical X error rate is determined as follows.

(1) **Preparing \mathcal{Q}_1 code states:** We simulate the preparation of $|\tilde{w}\rangle_{\mathcal{S}}$ and $|\tilde{w'}\rangle_{\mathcal{S'}}$ states, according to Section 5.2 (in case of error detection, we restart the preparation procedure until it completes). After the preparation completes, we know the frozen vectors $\mathbf{u}, \mathbf{u'} \in \{0, 1\}^{i-1}$, corresponding to the frozen sets \mathcal{Z} and $\mathcal{Z'}$, and the frozen vectors $\mathbf{v}, \mathbf{v'} \in \{0, 1\}^{N-i}$ corresponding to the frozen sets \mathcal{X} and $\mathcal{X'}$. Further, for $|\tilde{w}\rangle_{\mathcal{S}}$, we know the logical Z value w , and for $|\tilde{w'}\rangle_{\mathcal{S'}}$, we know the logical X value w' . Moreover, we also have the final errors e_X and e'_X on systems \mathcal{S} and $\mathcal{S'}$, respectively.

(2) **Generating the syndrome:** We generate the syndrome according to Steane's procedure (Fig. 4a). According to Lemma 3, the syndrome \mathbf{m} consists of a noise version of a random codeword of the classical polar code $P(N, \mathcal{Z}, \mathbf{u} \oplus \mathbf{u'})$. We generate \mathbf{m} as the sum of the random codeword from (2.1) and the two error terms from (2.2), below.

(2.2) First, we generate a **random codeword** $P_N(\mathbf{u} \oplus \mathbf{u'}, a', \mathbf{x'})$, by taking random values $a' \in \{0, 1\}$ and $\mathbf{x'} \in \{0, 1\}^{N-i}$.

(2.2) We then add to the generated codeword, the following **two error terms**¹³

- The first error term is $e_X \oplus e'_X$, where e_X and e'_X are given in step (1) (see (26)).
- The second term corresponds to the X error generated on the system $\mathcal{S'}$ during the implementation of the qubitwise $\text{CNOT}_{\mathcal{S} \rightarrow \mathcal{S'}}$, and the Pauli Z measurements on the system $\mathcal{S'}$.

Denoting the second error term above by e''_X , we may write,

$$\mathbf{m} = P_N(\mathbf{u} \oplus \mathbf{u'}, a', \mathbf{x'}) \oplus e_X \oplus e'_X \oplus e''_X \quad (88)$$

Further, we also update e_X , the error on system \mathcal{S} , by adding the X error generated on the system \mathcal{S} during the implementation of the qubitwise $\text{CNOT}_{\mathcal{S} \rightarrow \mathcal{S'}}$.

(3) **Error correction:** Given the frozen value $\mathbf{u} \oplus \mathbf{u'}$ from step (1), and the extracted syndrome \mathbf{m} from step (2), we use SC decoding to get an estimate $\hat{a'} \in \{0, 1\}$ of a' , and then generate

¹³In addition to the preparation errors (i.e., e_X and e'_X) considered in Lemma 3, we also consider here error generated by the qubitwise $\text{CNOT}_{\mathcal{S} \rightarrow \mathcal{S'}}$ and the Pauli Z measurements, within the Steane's error correction procedure.

an estimate of the total error $e_X^{\text{tot}} := e_X \oplus e'_X \oplus e''_X$, as follows

$$\hat{e}_X^{\text{tot}} = P_N(m) \oplus (\mathbf{u} \oplus \mathbf{u}', \hat{a}', \mathbf{0}). \quad (89)$$

Note that we do not need to estimate \mathbf{x}' here, since the induced logical error corresponds to an X -type stabilizer operator, acting trivially on the code space (see also the discussion after Lemma 3).

We then perform error correction on the state of the system S , and update the X error on S , by adding the estimated total error \hat{e}_X^{tot} .

(4) Guessing the logical value: The error correction is successful if we can successfully recover the logical Z value from the state of the system S , after error correction.

To get the logical Z value, we need to perform single-qubit Pauli Z measurements on system S , and then estimate the logical value from the measurement outcome.

It can be seen that the measurement outcome of Pauli Z measurements gives a noisy version of a random codeword of the classical polar code $P(N, \mathcal{Z}, \mathbf{u} \oplus \mathbf{u}')$, as follows,

$$\mathbf{m} = P_N(\mathbf{u} \oplus \mathbf{u}', w, \mathbf{x}) \oplus e_X \oplus e_X^m, \quad (90)$$

where w is the logical Z value corresponding to the initial state on the system S , \mathbf{x} is a random vector, e_X is the X error on the system S the after error correction in step (3), and e_X^m is the error caused by the single-qubit Pauli Z measurements on system S .

From the frozen vector $\mathbf{u} \oplus \mathbf{u}'$ and the noisy codeword \mathbf{m} in (90), we generate an estimate \hat{w} of w , using the SC decoding. If $\hat{w} \neq w$, we report a decoding failure, otherwise decoding succeeds.

We run the above steps (1)-(4), until we report $f > 0$ decoding failures. Let R be the number of runs for f decoding failures, then the logical X error rate, denoted by P_X^L , is computed as follows,

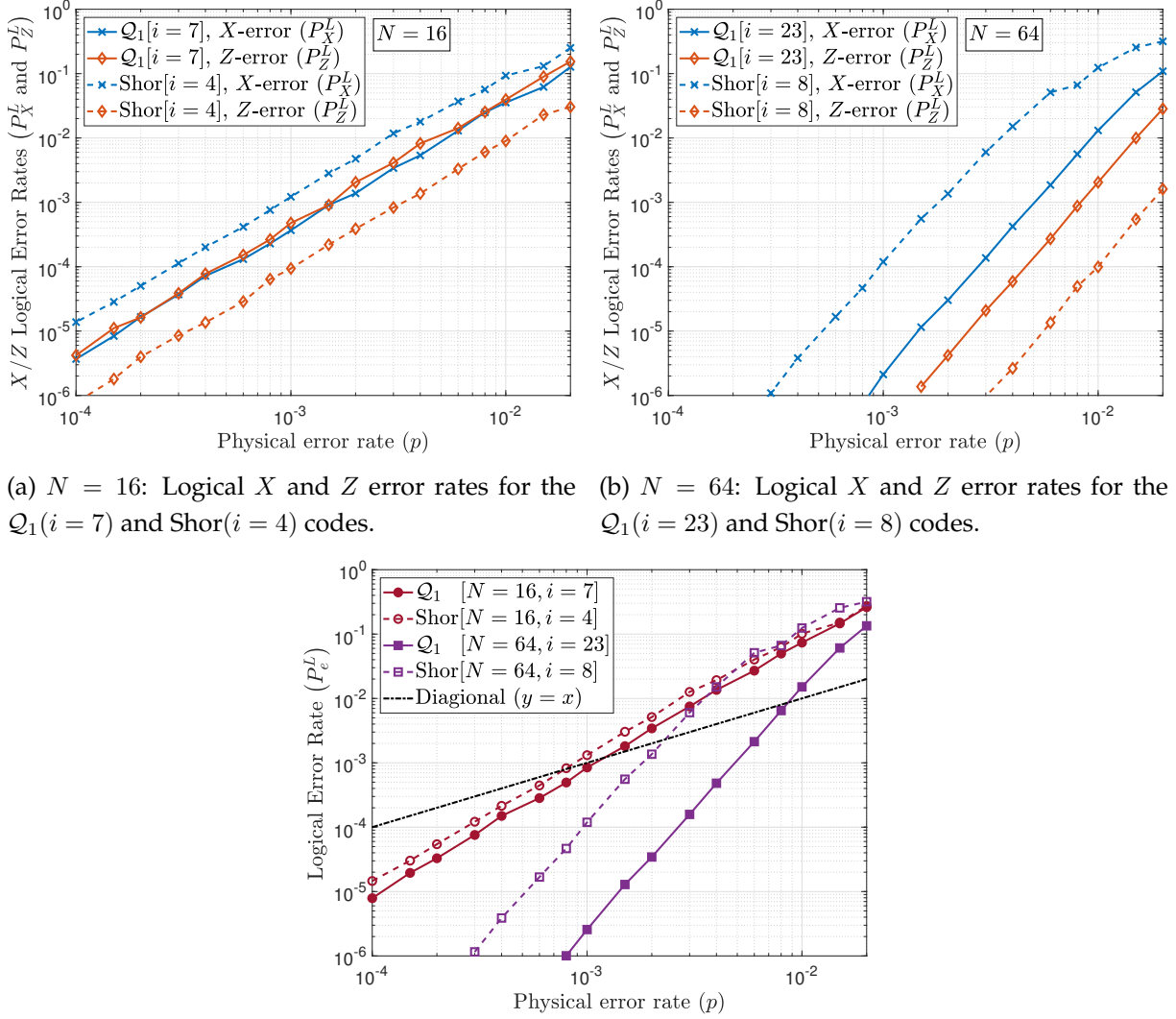
$$P_X^L = \frac{f}{R}. \quad (91)$$

For our numerical simulations, the value of f varies between 50 to 200, depending on the physical error rate p in Section 5.1.

Logical Z Error Rate. To determine the logical Z error rate, we consider a logical Pauli X basis code state $|\tilde{w}\rangle_S = Q_N(|\mathbf{u}\rangle_{\mathcal{Z}} \otimes |\bar{w}\rangle_{\mathcal{I}} \otimes |\bar{\mathbf{v}}\rangle_{\mathcal{X}})$, $w \in \{0, 1\}$, that we want to protect against Z errors. Further, we consider a logical Pauli Z basis code state $|\tilde{w}'\rangle_{S'} = Q_N(|\mathbf{u}'\rangle_{\mathcal{Z}'} \otimes |w'\rangle_{\mathcal{I}'} \otimes |\bar{\mathbf{v}'}\rangle_{\mathcal{X}'})$, $w' \in \{0, 1\}$, to be used as the ancilla system for syndrome extraction (Fig. 4b.) The logical Z error rate is then determined similarly to the above procedure for logical X error rate, while inverting X and Z bases, and using Lemma 4 instead of Lemma 3. The logical Z error rate is denoted by P_Z^L .

Finally, the logical error rate (accounting for both X and Z errors), denoted by P_e^L , is given as follows,

$$P_e^L = P_X^L + P_Z^L - P_X^L P_Z^L. \quad (92)$$



(c) Logical error rate P_e^L for \mathcal{Q}_1 and Shor codes of length $N = 16$ and $N = 64$.

Fig. 14: Logical error rate P_X^L , P_Z^L , and P_e^L , for \mathcal{Q}_1 and Shor codes of length $N = 16$ and $N = 64$.

Numerical Results. We provide numerical results for both \mathcal{Q}_1 and Shor- \mathcal{Q}_1 codes, of length $N = 16$ and $N = 64$ qubits.

\mathcal{Q}_1 codes: We consider the two \mathcal{Q}_1 codes with $(N = 16, i = 7)$ and $(N = 64, i = 23)$, from the previous section.

Shor codes: We consider the two Shor codes with $(N = 16, i = 4)$ and $(N = 64, i = 8)$, from Table 1.

In Fig. 14, we plot logical error rate values P_X^L , P_Z^L , and P_e^L , with respect to the physical error rate p . First, in Fig. 14a, we plot logical X and Z error rates (P_X^L and P_Z^L), for the \mathcal{Q}_1 and Shor codes of length $N = 16$. Logical X and Z error rates are almost the same for the \mathcal{Q}_1 code, while a clear imbalance may be observed for the Shor code. As we need to correct both types of error, for the Shor code, the total logical error rate value P_e^L becomes dominated by P_X^L . Hence, the \mathcal{Q}_1 code, whose construction has been optimized with respect to the P_e^L value (Section 3.2), is better suited to the depolarizing noise model considered here. Similar observations hold for

the \mathcal{Q}_1 and Shor codes of length $N = 16$, in Fig. 14b. However, we note that in this case, even the \mathcal{Q}_1 code fails to achieve a perfect balance between logical X and Z error rates. Finally, in Fig. 14c, we plot the total logical error rate P_e^L for the two \mathcal{Q}_1 and the two Shor codes, of length $N = 16$ and $N = 64$. A clear advantage of the \mathcal{Q}_1 code may be observed, especially for $N = 64$.

From Fig. 14c we may also compute the *pseudothresholds* [41, 42] of these codes, defined by the crossing point between the diagonal line ($y = x$) and the logical error rate curve. If the physical error rate p falls below the pseudothreshold, then the code is guaranteed to lower the logical error rate below p ($P_e^L < p$). It can be observed that the pseudothreshold of the $\mathcal{Q}_1(N = 16, i = 7)$ code is $p_{\text{th}} \approx 0.001$, while for the $\mathcal{Q}_1(N = 64, i = 23)$ code, we get $p_{\text{th}} \approx 0.009$.

6 Conclusion

Polar encoded quantum computation may be seen as an error correction centric approach to FTQC. It exploits a family of codes that have met with remarkable success, fueled by their excellent error correction performance, under practical, low complexity decoding. In this paper, we focused on two closely related ingredients of FTQC, namely fault-tolerant code state preparation and fault-tolerant error correction. We considered polar codes encoding one logical qubit, referred to as \mathcal{Q}_1 codes, constituting a case of practical interest to FTQC (they support transversal logical CNOT gate), and which we showed to be a meaningful generalization of the well-known Shor codes.

We proposed a measurement-based procedure to prepare logical \mathcal{Q}_1 code states, where two-qubit Pauli measurements are applied recursively, on equivalent code states. The number of recursion levels, thus the number of time steps required to implement the proposed procedure, is logarithmic in the number of qubits. We further showed that our procedure can be made fault-tolerant, by incorporating an error detection mechanism, exploiting the redundancy in the measurement outcomes, at each level of recursion. Finally, we integrated the proposed fault-tolerant code state preparation into the Steane error correction procedure, and provided numerical estimates of the logical error rates for \mathcal{Q}_1 and Shor codes of length 16 and 64 qubits, assuming a circuit-level depolarizing noise model. Our numerical results showed that \mathcal{Q}_1 codes significantly outperforms Shor codes, for the same code length and minimum distance. The gap between \mathcal{Q}_1 and Shor codes is expected to increase with the codelength, due to the \mathcal{Q}_1 codes construction that effectively exploits the channel polarization property.

To prepare longer \mathcal{Q}_1 code states, a possible approach is to replace the error detection mechanism incorporated in the preparation procedure, by an error correction one (ongoing work). This would allow correcting errors on the fly, rather than just detecting them, thus avoiding restarting the preparation procedure from the beginning.

Acknowledgment

This work was supported by the QuantERA grant EQUIP, by the French Agence Nationale de la Recherche, ANR-22-QUA2-0005-01.

References

- [1] John Preskill. Fault-tolerant quantum computation. In *Introduction to quantum computation and information*, pages 213–269. World Scientific, 1998.
- [2] Daniel Gottesman. An introduction to quantum error correction and fault-tolerant quantum computation. In *Quantum information science and its contributions to mathematics, Proceedings of Symposia in Applied Mathematics*, volume 68, pages 13–58, 2010.
- [3] Daniel Gottesman. *Stabilizer codes and quantum error correction*. PhD thesis, California Institute of Technology, 1997.
- [4] Peter W Shor. Fault-tolerant quantum computation. In *Proceedings of 37th Conference on Foundations of Computer Science (FOCS)*, pages 56–65. IEEE, 1996.
- [5] David P DiVincenzo and Peter W Shor. Fault-tolerant error correction with efficient quantum codes. *Physical review letters*, 77(15):3260, 1996.
- [6] Andrew M Steane. Active stabilization, quantum computation, and quantum state synthesis. *Physical Review Letters*, 78(11):2252, 1997.
- [7] Andrew M Steane. Fast fault-tolerant filtering of quantum codewords. *arXiv quant-ph/0202036*, 2002.
- [8] Emanuel Knill. Scalable quantum computing in the presence of large detected-error rates. *Physical Review A*, 71(4):042322, 2005.
- [9] A Yu Kitaev. Fault-tolerant quantum computation by anyons. *Annals of Physics*, 303(1), 2003.
- [10] Hector Bombin and Miguel Angel Martin-Delgado. Topological quantum distillation. *Physical review letters*, 97(18):180501, 2006.
- [11] Austin G Fowler, Matteo Mariantoni, John M Martinis, and Andrew N Cleland. Surface codes: Towards practical large-scale quantum computation. *Physical Review A*, 86(3):032324, 2012.
- [12] Andrew J Landahl, Jonas T Anderson, and Patrick R Rice. Fault-tolerant quantum computing with color codes. *arXiv:1108.5738*, 2011.
- [13] Vivien Londe and Anthony Leverrier. Golden codes: quantum LDPC codes built from regular tessellations of hyperbolic 4-manifolds. *Quantum Information and Computation*, 19(5-6):361–391, 2019.
- [14] Jean-Pierre Tillich and Gilles Zémor. Quantum LDPC codes with positive rate and minimum distance proportional to the square root of the blocklength. *IEEE Transactions on Information Theory*, 60(2):1193–1202, 2013. arXiv:0903.0566.
- [15] Daniel Gottesman. Fault-tolerant quantum computation with constant overhead. *Quantum Information & Computation*, 14(15-16):1338–1372, 2014.

- [16] Matthew B Hastings, Jeongwan Haah, and Ryan O’Donnell. Fiber bundle codes: Breaking the $N^{1/2}$ polylog(N) barrier for quantum LDPC codes. *arXiv:2009.03921*, 2020.
- [17] Nikolas P Breuckmann and Jens N Eberhardt. Balanced product quantum codes. *arXiv:2012.09271*, 2020.
- [18] Pavel Panteleev and Gleb Kalachev. Asymptotically good quantum and locally testable classical LDPC codes. *arXiv:2111.03654*, 2021.
- [19] Anthony Leverrier and Gilles Zémor. Quantum Tanner codes. *arXiv:2202.13641*, 2022.
- [20] David Poulin and Yeojin Chung. On the iterative decoding of sparse quantum codes. *Quantum Information and Computation*, 8(10):987–1000, 2008.
- [21] Omar Fawzi, Antoine Grospellier, and Anthony Leverrier. Efficient decoding of random errors for quantum expander codes. In *Proceedings of the 50th Annual ACM SIGACT Symposium on Theory of Computing*, pages 521–534, 2018.
- [22] Ye-Hua Liu and David Poulin. Neural belief-propagation decoders for quantum error-correcting codes. *Physical review letters*, 122(20):200501, 2019.
- [23] Nicolas Delfosse and Naomi H Nickerson. Almost-linear time decoding algorithm for topological codes. *Quantum*, 5:595, 2021.
- [24] Joschka Roffe, David R White, Simon Burton, and Earl Campbell. Decoding across the quantum low-density parity-check code landscape. *Physical Review Research*, 2(4):043423, 2020. *arXiv:2005.07016*.
- [25] Pavel Panteleev and Gleb Kalachev. Degenerate quantum LDPC codes with good finite length performance. *Quantum*, 5:585, 2021. *arXiv:1904.02703*.
- [26] Julien Du Crest, Mehdi Mhalla, and Valentin Savin. Stabilizer inactivation for message-passing decoding of quantum LDPC codes. In *Proc. of IEEE Information Theory Workshop (ITW)*, 2022. *arXiv:2205.06125*.
- [27] Shouzhen Gu, Christopher A Pattison, and Eugene Tang. An efficient decoder for a linear distance quantum LDPC code. *arXiv preprint arXiv:2206.06557*, 2022.
- [28] Anthony Leverrier and Gilles Zémor. Efficient decoding up to a constant fraction of the code length for asymptotically good quantum codes. *arXiv preprint arXiv:2206.07571*, 2022.
- [29] Irit Dinur, Min-Hsiu Hsieh, Ting-Chun Lin, and Thomas Vidick. Good quantum LDPC codes with linear time decoders. *arXiv preprint arXiv:2206.07750*, 2022.
- [30] Adam Holmes, Mohammad Reza Jokar, Ghasem Pasandi, Yongshan Ding, Massoud Pe-dram, and Frederic T Chong. NISQ+: Boosting quantum computing power by approximating quantum error correction. *arXiv:2004.04794*, 2020.
- [31] Erdal Arıkan. Channel polarization: A method for constructing capacity-achieving codes for symmetric binary-input memoryless channels. *IEEE Transactions on Information Theory*, 55(7):3051–3073, 2009.

- [32] Joseph M. Renes, Frédéric Dupuis, and Renato Renner. Efficient polar coding of quantum information. *Physical Review Letters*, 109(5):050504, August 2012.
- [33] Mark M. Wilde and Saikat Guha. Polar codes for degradable quantum channels. *IEEE Transactions on Information Theory*, 59(7):4718–4729, July 2013.
- [34] Joseph M. Renes and Mark M. Wilde. Polar codes for private and quantum communication over arbitrary channels. *IEEE Transactions on Information Theory*, 60(6):3090–3103, June 2014.
- [35] Frédéric Dupuis, Ashutosh Goswami, Mehdi Mhalla, and Valentin Savin. Polarization of quantum channels using Clifford-based channel combining. *IEEE Transactions on Information Theory*, 67(5):2857–2877, 2021. arXiv:1904.04713.
- [36] Anirudh Krishna and Jean-Pierre Tillich. Magic state distillation with punctured polar codes. *arXiv preprint arXiv:1811.03112*, 2018.
- [37] Peter W Shor. Scheme for reducing decoherence in quantum computer memory. *Physical review A*, 52(4):R2493, 1995.
- [38] Dave Bacon. Operator quantum error-correcting subsystems for self-correcting quantum memories. *Physical Review A*, 73(1):012340, 2006.
- [39] Ido Tal and Alexander Vardy. How to construct polar codes. *IEEE Transactions on Information Theory*, 59(10):6562–6582, 2013.
- [40] John Napp and John Preskill. Optimal Bacon-Shor codes. *Quantum Information and Computation*, 13:490–510, 2013.
- [41] Krysta M Svore, Andrew W Cross, Isaac L Chuang, and Alfred V Aho. A flow-map model for analyzing pseudothresholds in fault-tolerant quantum computing. *Quantum Information & Computation*, 6(3):193–212, 2006.
- [42] Yu Tomita and Krysta M Svore. Low-distance surface codes under realistic quantum noise. *Physical Review A*, 90(6):062320, 2014.